Title: **Pannexin 3 channels regulate architecture, adhesion, barrier function and inflammation in the skin**

Authors: **Brooke L. O'Donnell[1], Rafael E. Sanchez-Pupo[1], Samar Sayedyahossein[2], Mehdi Karimi[3], Mehrnoosh Bahmani[4], Christopher Zhang[1], Danielle Johnston[1], John Kelly[1], C. Brent Wakefield[1,5], Kevin Barr[1], Lina Dagnino[2] and Silvia Penuela[1,5,6]**

Affiliations:

[1]Department of Anatomy and Cell Biology, Schulich School of Medicine and Dentistry, University of Western Ontario, London, Ontario, Canada, N6A 5C1.

[2]Department of Physiology and Pharmacology, Schulich School of Medicine and Dentistry, University of Western Ontario, London, Ontario, Canada, N6A 5C1.

[3]Department of Mathematics, Illinois State University, Normal, Illinois, United States, 61790.

[4]Ontario College of Pharmacists, Toronto, Ontario, Canada, M5R 2R4.

[5]Western's Bone and Joint Institute, The Dr. Sandy Kirkley Centre for Musculoskeletal Research, University Hospital, London, Ontario, Canada, N6G 2V4.

[6]Department of Oncology, Division of Experimental Oncology, Schulich School of Medicine and Dentistry, University of Western Ontario, London, Ontario, Canada, N6A 5C1.

*Corresponding author: Silvia Penuela, Associate Professor, Department of Anatomy and Cell Biology, University of Western Ontario, London, Ontario, Canada. Tel. 519-661-2111 ext. 84735; E-mail: spenuela@uwo.ca

Running title: PANX3 required for skin homeostasis with aging

Keywords: Pannexins, PANX3, skin, keratinocyte, knockout mouse, adhesion, barrier function, inflammation

Summary

Pannexin 3 is a new regulator of skin structure and function. Here, O'Donnell *et al.* demonstrate its role in the maintenance of proper skin architecture with aging, epidermal barrier function, inflammation, and keratinocyte adhesion through Wnt signalling and E-cadherin stabilization.

Abstract
The channel-forming glycoprotein Pannexin 3 (PANX3) functions in cutaneous wound healing and keratinocyte differentiation, but its role in skin homeostasis through aging is not yet understood. We found that PANX3 is absent in newborn skin but becomes upregulated with age. We characterized the skin of global *Panx3* knockout mice (KO) and found that KO dorsal skin showed sex-differences at different ages, but generally had reduced dermal and hypodermal areas compared to aged-matched controls. Transcriptomic analysis of KO epidermis revealed reduced E-cadherin stabilization and Wnt signalling compared to WT, consistent with the inability of primary KO keratinocytes to adhere in culture, and diminished epidermal barrier function in KO mice. We also observed increased inflammatory signalling in KO epidermis and higher incidence of dermatitis in aged KO mice compared to wildtype controls. These findings suggest that during skin aging, PANX3 is critical in the maintenance of dorsal skin architecture, keratinocyte cell-cell and cell-matrix adhesion and inflammatory skin responses.

Introduction

Discovered in 2000, pannexins (PANX1, PANX2, PANX3) are a family of channel-forming glycoproteins (Panchin et al., 2000) whose primary function is to form large-pore, single-membrane channels to allow the passage of ions and metabolites during autocrine and paracrine signalling (Bao et al., 2004; Chekeni et al., 2011; Ishikawa et al., 2011; Iwamoto et al., 2010; Locovei et al., 2006; Pelegrin and Surprenant, 2006). Although PANX1 shows a widespread expression pattern, PANX2 and PANX3 localization seem to be more restricted, but interestingly, all three pannexins are found in the skin (Le Vasseur et al., 2014; Penuela et al., 2007).

To date, PANX3 has been reported in cartilage (Iwamoto et al., 2010), teeth (Fu et al., 2015), bone (Ishikawa et al., 2011), skeletal muscle (Langlois et al., 2014), skin (Penuela et al., 2007), adipose (Pillon et al., 2014; Wakefield et al., 2021), mammary glands (Bond et al., 2011), a subset of blood vessels (Lohman et al., 2012), the small intestine (Bond et al., 2011) and the male reproductive tract (Turmel et al., 2011). In chondrocytes and osteoblasts, PANX3 is induced during the differentiation process and functions at the cell surface as an ATP release channel and/or in the endoplasmic reticulum (ER) as a Ca^{2+} leak channel (Ishikawa et al., 2014; Ishikawa et al., 2011; Iwamoto et al., 2010). Furthermore, PANX3 is a mechanosensitive channel, capable of sulforhodamine B dye uptake after mechanical stimulation in ectopically expressing rat epidermal keratinocytes (REKs), but the structure and stoichiometry of the channel has not yet been elucidated (Celetti et al., 2010; O'Donnell and Penuela, 2021).

Our group has previously demonstrated the regulation of PANX1 throughout skin development and its role in the establishment of proper skin structure. PANX1 is highly expressed in young mouse dorsal skin, specifically in keratinocytes and fibroblasts, but becomes downregulated with age. Moreover, when comparing the dorsal skin architecture of wildtype (WT) global *Panx1* knockout (KO) mice, we discovered that *Panx1* KO dorsal skin has a significantly reduced dermal and increased hypodermal area as well as compromised wound healing abilities and increased fibrotic scarring compared to age-matched controls (Penuela et al., 2014). However, the role of PANX3 in skin homeostasis during aging is unknown.

PANX3 protein was first detected in the skin by Penuela *et al.* (2007) in 3-week-old C57BL/6 mice, and was found to be present in all epidermal layers of both thin and thick skin as well as keratin-expressing sebocytes with a predominantly intracellular localization (Celetti et al., 2010). Similarly in human skin, PANX3 exhibits an intracellular localization pattern in all layers

of the epidermis (Penuela et al., 2007) and in supporting structures such as sebaceous glands, eccrine glands, hair follicles and blood vessels (Cowan et al., 2012). PANX3 can be detected in the epidermis and underlying cells as early as E13.5 (Celetti et al., 2010), but there are conflicting results as to whether its expression remains consistent past birth. Earlier reports claim PANX3 is undetectable in newborn skin (Celetti et al., 2010), but others found both unphosphorylated and Ser68 phosphorylated PANX3 in newborn skin (Ishikawa et al., 2019). Thus, the regulation of PANX3 levels with skin aging remains to be determined.

Within the epidermis, PANX3 has been implicated in the process of keratinocyte differentiation and the establishment of proper epidermal structure. Global *Panx3* KO mice were shown to have a reduced epidermal and dermal thickness at P4, but these phenotypes were no longer present at P10, P20 and P38, and P4 *Panx3* KO skin also showed marked reduction in keratinocyte differentiation markers. Furthermore, when PANX3 was overexpressed in the HaCaT human keratinocytic cell line, PANX3 increased keratinocyte differentiation, inducing the expression of gene drivers of the keratinocyte differentiation program such as Epiprofin and Notch1. At the same time ectopic PANX3 expression reduced proliferation by promoting keratinocyte arrest in the G_0/G_1 phase. This was achieved through protein kinase B/nuclear factor of activated T-cells (Akt/NFAT) signalling triggered by PANX3 function as an ATP and Ca^{2+} release channel (Zhang et al., 2021).

Similar to *Panx1* KO mice, Zhang *et al.* (2019) also demonstrated that *Panx3* KO mice have delayed cutaneous wound healing capacities compared to heterozygous controls. PANX3 was found to be particularly important during re-epithelialization, where keratinocytes proliferate, migrate, and then differentiate to replace the lost epithelium via epithelial-to-mesenchymal transition (EMT) induction. Specifically, during TGF-β stimulated-EMT, PANX3 was found to act as both a cell surface and ER channel for the passage of ATP and Ca^{2+}, respectively, in PANX3-overexpressing HaCaT keratinocytes (Zhang et al., 2019). However, the function of PANX3 in skin homeostasis and aging in the absence of challenges such as wound healing has yet to be fully investigated.

Using the global *Panx3* KO mouse model previously developed and characterized by our group (Moon et al., 2015), we investigated PANX3 expression and function in the maintenance of proper skin architecture with aging as well as its action in the various cell types of the skin. PANX3 is undetectable at the protein level in dermal fibroblasts in the absence of any challenges to the skin but is highly expressed in keratinocytes where it is critical for keratinocyte adhesion. We found that PANX3 levels increase with aging and its presence is required to maintain proper skin structure, epidermal barrier function and inflammatory responses, with *Panx3* KO epidermis exhibiting impaired Wnt and E-cadherin signalling, a compromised barrier and increased incidence of dermatitis.

Results

PANX3 is upregulated in WT neonatal mouse dorsal skin

To determine the regulation of PANX3 levels throughout dorsal skin aging, both male (Fig. 1 A) and female (Fig. 1 B) WT dorsal skin were collected from multiple timepoints ranging from P0 to 1 year of age, with age-matched global *Panx3* KO mice run in parallel as the negative control. Both male and female dorsal skin were found to have the same PANX3 protein expression pattern, with PANX3 undetectable in newborn skin, becoming upregulated at P4 and remaining at high levels throughout all ages investigated. Due to the variation in glycosylation modifications, PANX3 bands appear as either a singlet or doublet in Western blots. In the doublet, the lower

species corresponds to the high mannose glycosylated form Gly1 and the higher species corresponds to the complex glycoprotein species Gly2 (Penuela et al., 2009). In the dorsal skin samples, the Gly1 species of PANX3 was present, consistent with previous research which indicates PANX3 has a predominantly intracellular localization in the epidermis and adnexal skin structures such as blood vessels, eccrine sweat glands, hair follicles and sebaceous glands (Celetti et al., 2010; Cowan et al., 2012). Additionally, background level staining was present in *Panx3* KO and P0 WT dorsal skin samples due to the polyclonal nature of the anti-PANX3 CT-379 antibody used. To more closely examine the increase in PANX3 levels at the early postnatal days, P2 dorsal skin was also collected and analyzed via immunoblotting, where we found a gradual increase in PANX3 levels from P0 to P4 (Fig. 1 C; full blots in Fig. S1 A-C). These findings suggest, that although absent in newborn mice, PANX3 is present in neonatal dorsal skin and its expression persists with skin aging.

Since it is known that all pannexins are present in WT skin at P4 (Abitbol et al., 2019; Penuela et al., 2014; Sanchez-Pupo et al., 2022), both PANX1 and PANX2 levels were investigated in P4 WT and *Panx3* KO neonatal skin to test for any potential compensation from the other family pannexin family members. We found at this age, PANX1 levels were similar between P4 WT and *Panx3* KO dorsal skin (Fig. S2 A). Total PANX2 levels (full length and isoform 202) did not differ between genotypes, but interestingly, the levels of the shorter PANX2 isoform 202 were significantly reduced in *Panx3* KO mice (Fig. S2 B). Full length PANX2 was also quantified in the dorsal skin samples and was not significantly different between genotypes. At the mRNA level, no differences were seen in *Panx1*, *Panx2* full length or *Panx2* isoform 202 transcripts (Fig. S2 C), indicating that overall, only PANX2 isoform 202 protein levels are reducedwith *Panx3* ablation in dorsal skin.

***Panx3* KO mice have reduced dorsal skin thickness at different ages in males and females, but no changes in paw skin epidermal architecture**

The global *Panx3* KO mice used in this study do not show any overt phenotypes in thin or thick skin; however, upon closer histological examination *Panx3* KO dorsal skin exhibits sex-specific architectural differences compared to WT mice at multiple ages. In male dorsal skin (Fig. 2), the hypodermal area of *Panx3* KO mice at 4 weeks was significantly reduced compared to age-matched controls, but this was not seen in neonatal or 22-week-old mice. Additionally, at 1 year, *Panx3* KO mice showed both a reduced epidermal and dermal area as well as a reduced hypodermal area compared to WT dorsal skin. However, female dorsal skin (Fig. 3) of *Panx3* KO mice had significantly reduced hypodermal areas from P0 to 1 year, but a reduced epidermal and dermal area was only observed in P0 and 1-year-old *Panx3* KO mice compared to WT controls. Contrarily, there were no significant differences seen in the epidermal area of both male (Fig. S3 A) and female (Fig. S4 A) WT and *Panx3* KO paw skin at P4, 4 weeks and 22 weeks of age. Since PANX3 has been shown to be a mechanosensitive channel (Celetti et al., 2010; Penuela et al., 2007), we challenged the paws through repeated mechanical impact and increased abrasion from controlled treadmill exercise to determine the impact of *Panx3* ablation on the epidermis of murine thick skin. However, even after a 6-week treadmill running program, no differences were observed in the epidermal area of the paw skin regardless of exercise treatment or genotype (Fig. S3 B, Fig. S4 B). Taken together, these results demonstrate that PANX3 is required for the maintenance of proper dorsal skin architecture, particularly in aged skin, but may not be essential in the conservation of thick skin epidermal structure in basal or challenged conditions.

PANX3 is undetectable in cultured WT dermal fibroblasts and its transcript levels are unchanged by TGF-β stimulation

To further investigate the structural phenotypes seen in *Panx3* KO dorsal skin, we took a closer examination of the individual layers of the skin, beginning with the dermis. Through histological measurements we determined that the significant reduction seen in the epidermal and dermal area of P0 female *Panx3* KO skin was due to a reduction in the dermal area (Fig. 4 A). To examine fibroblast PANX3 expression and cellular properties we isolated and cultured primary fibroblasts from neonatal dorsal skin. The isolated dermal fibroblasts from each genotype could be cultured and passaged with no signs of adherence or growth deficits. However, PANX3 protein was undetectable in cultured WT and *Panx3* KO dermal fibroblasts (Fig. 4 B; full blot in Fig. S1 D) but was present at the transcript level in WT cells albeit at very low levels (Fig. 4 C). Additionally, when WT dermal fibroblasts were activated using TGF-β stimulation, confirmed by a corresponding increase in α-smooth muscle actin (*Acta2*) transcripts, *Panx3* mRNA levels remained unchanged in control and TGF-β treated conditions (Fig. 4 C). We also performed a Masson's Trichrome stain which stains collagen blue as a proxy for dermal fibroblast function, since these cells secrete collagen that makes up much of the extracellular matrix in the dermis (Fig. 4 D). However, visually there were similar levels of collagen in the dorsal skin of male mice at 4-weeks of age from each genotype, consistent with the histology assessments shown in Fig. 2. Overall, these findings suggest that PANX3 is present at negligible levels in dermal fibroblasts in the absence of challenges to the skin such as wound repair (Zhang et al., 2019).

***Panx3* KO neonates have compromised epidermal barrier function**

Previously, PANX3 function has been investigated in REK or HaCaT keratinocyte cell line overexpression systems, but no studies have explored the effects of endogenous PANX3 in keratinocytes (Celetti et al., 2010; Zhang et al., 2021; Zhang et al., 2019). Thus, we isolated the epidermis of P4 WT and *Panx3* KO mice to investigate endogenous PANX3 expression and the effect of *Panx3* ablation in these cells. We identified that, unlike in dermal fibroblasts, *Panx3* transcripts were highly expressed in the WT neonatal epidermis and absent in the KO (Fig. 5 A). However, histological measurements showed no significant differences in the epidermal area between WT and *Panx3* KO dorsal skin of both sexes (Fig. 5 B).

In the epidermis, keratinocytes adhere to the basement membrane through cell-matrix attachments as well as other keratinocytes via cell-cell attachments to establish an impermeable barrier as a critical layer of protection from pathogens and water loss (Baroni et al., 2012). To investigate whether cell-cell adhesion is altered in *Panx3* KO mice, a toluidine blue dye assay was performed using P2 *Panx3* KO and WT mice to test for epidermal barrier function. Both male and female *Panx3* KO pups immersed in the dye solution had blue staining on all areas of the skin, indicating dye permeation, not seen in WTs or unstained controls. Additionally, prominent blue staining was observed in the mouth/nose area, paws and tails of *Panx3* KO mice (Fig. 5 C). Ultimately, these findings uncovered a novel phenotype of *Panx3* KO mice, demonstrating that KO skin exhibits a leaky epidermal barrier and reduced keratinocyte cell-cell adhesion.

Analysis of WT and *Panx3* KO neonatal epidermis transcriptomes

To understand the signalling mechanisms behind the compromised epidermal barrier upon *Panx3* deletion, we performed a Clariom™ S transcriptomic profiling analysis of WT and KO neonatal epidermis. Dorsal skin was dissected from P4 pups, incubated with dispase to separate the

epidermis from the underlying skin layers, digested with trypsin to break up cell contacts, pooled from multiple pups and flash frozen for RNA isolation (Fig. 6 A). The transcriptomic expression profiles were analyzed by Transcriptome Analysis Console (TAC) and RStudio Cloud software to create lists of differentially expressed genes (DEGs) with gene-level fold change of minimum ±1.5 and $p < 0.05$ significance. Of the 22,206 genes tested, 999 DEGs were identified with 539 upregulated and 460 downregulated genes in the *Panx3* KO neonatal epidermis. Initial quality control using a principal component analysis concluded samples from each genotype were clearly separated along each axis, whereas samples within the same genotype clustered together (Fig. 6 B). A heat map shows the first thirty differentially ranked genes with a gene-level fold change of ±2 between WT and *Panx3* KO neonatal epidermis, with *Panx3* transcript levels being the most significantly reduced in the KO samples, as an internal control (Fig. 6 C). From the DEGs list, gene candidates with altered expression were organized into functional categories and signalling pathways relevant in skin health and skin conditions such as psoriasis, dermatitis, and skin cancer (Fig 6 D). Consistent with our findings of altered skin structure and barrier function, many gene candidates differentially expressed in WT and KO neonatal epidermis were implicated in skin development and barrier function. Alterations in wound healing, hair follicles, differentiation and proliferation genes also reflected previous findings (Zhang et al., 2021; Zhang et al., 2019).

Keratinization and epidermal barrier function signalling is altered in KO neonatal epidermis

We first investigated the functional category of differentiation since PANX3 was implicated in keratinocyte differentiation previously (Celetti et al., 2010; Zhang et al., 2021; Zhang et al., 2019), and the sequential differentiation of keratinocytes is required for the establishment and maintenance of the epidermal barrier (Wikramanayake et al., 2014). Gene Set Enrichment Analysis (GSEA) was performed to identify statistically significant changes in *a priori* defined gene sets and pathways using the Molecular Signatures Database (MSigDB) C2 collection of 2922 gene sets. The gene set for keratinization was one of the most positively enriched in *Panx3* KO neonatal epidermis compared to WT (Fig. 7 A). Interestingly, all upregulated keratins and keratin-associated proteins have restricted expression in hair follicles (Bragulla and Homberger, 2009). Similarly, Reactome pathway analysis using minimum 1.5-fold change gene lists identified keratinization as the most enriched pathway ($p = 4.90 \times 10^{-12}$). Keratinization is the formation and polymerization of keratins into intermediate filaments which is involved in many processes in the epidermis including keratinocyte differentiation and the formation and maintenance of the epidermal barrier (Smack et al., 1994). To assess the differentiation status of both WT and *Panx3* KO neonatal epidermis, transcript levels of both basal/undifferentiated keratin 14 and 5 (*K14, K5*) and suprabasal/differentiated loricrin and involucrin (*Lor, Inv*) keratinocyte markers were analyzed, but no significant differences were observed between genotypes (Fig. 7 B). When primary WT keratinocytes were differentiated by calcium treatment, as evidenced by an increase in keratin 10 (*K10*) transcripts, (mRNA) *Panx3* levels remained unchanged between control and calcium conditions (Fig. 7 C). Using STRING analysis, we noticed that many of the altered genes functioned specifically in the formation and maintenance of the epidermal barrier. One cluster specifically, was found to be associated with not only keratinization, but also epidermis morphogenesis and formation of the cornified envelope (Fig. 7 D). Formation of cornified envelope was also the second-most enriched pathway found with Reactome Pathway analysis ($p = 3.84 \times 10^{-05}$). The normalized expression of gene candidates associated with epidermal barrier function such as epithelial splicing regulatory protein 2 (*Esrp2*), late cornified envelope 1m (*Lce1m*), cornifin-B (*Sprr1b*) and filaggrin 2 (*Flg2*) were either significantly reduced or trended

to a decrease in KO neonatal epidermis compared to WT (Fig 7 E). Thus, although keratinization has many functions in epidermal homeostasis, our findings suggest that most differentially expressed genes in KO neonatal epidermis were critical in epidermal barrier function which is consistent with the phenotypes observed.

Panx3 KO neonatal epidermis has negatively enriched adhesion signalling, and KO keratinocytes do not adhere in culture

Cell-cell attachments such as tight junctions, adherens junctions and desmosomes are also critical in forming and maintaining the structural integrity of the epidermal barrier (Baroni et al., 2012). Using GSEA, gene sets for E-cadherin stabilization and Wnt signalling (Fig. 8 A) pathways—critical pathways in keratinocyte adhesion, specifically at adherens junctions (Hartsock and Nelson, 2008; Valenta et al., 2012)—were the most negatively enriched in *Panx3* KO neonatal epidermis compared to WT. To corroborate these findings, a few of the downregulated genes identified within each gene set (chosen based on fold change in KO versus WT) were selected to compare the relative transcript levels between the neonatal epidermis of each genotype. Decreased cadherin 1 (*Cdh1*), vinculin (*Vcl*), Wnt family member 3 (*Wnt3*) and low-density lipoprotein receptor-related protein 5 (*Lrp5*) transcripts were seen in *Panx3* KO neonatal epidermis compared to controls, but only *Vcl*, *Wnt3* and *Lrp5* transcript levels were significantly reduced (Fig. 8 B).

To explore whether the negatively enriched adhesion signalling in the KO epidermis was reflected in the cultured keratinocytes, we first isolated and cultured WT and *Panx3* KO primary keratinocytes from P4 dorsal skin (Fig. 6 A) to assess for cell-matrix adhesion. WT keratinocytes adhered to the culture dish and spread out to make contacts with neighbouring keratinocytes to form clusters. In contrast, *Panx3* KO keratinocytes did not adhere to tissue culture plastic or contact neighbouring cells, remaining ‘balled up’ in structure and appeared to lift off the plate shortly after isolation (Fig. 8 C). However, we verified that this phenotype was not due to reduced *Panx3* KO keratinocyte viability, since there were no significant differences in live and dead cell percentages, as determined by trypan blue exclusion assay, between the neonatal epidermis of each genotype before plating (Fig. 8 D). This phenotype was also independent of the extracellular matrix protein used for culturing since *Panx3* KO keratinocytes exhibited the same low adherence when isolated and plated onto surface-treated culture plates coated with 50 ug/mL collagen, 100 ug/mL collagen, laminin or fibronectin (Fig. 8 D). Ultimately, these results indicate that *Panx3* KO keratinocytes show both cell-cell and cell-matrix adhesion deficits, reflected in their reduced E-cadherin and Wnt signalling, inability of primary KO keratinocytes to adhere in culture and the compromised epidermal barrier in KO neonates.

Aged *Panx3* KO mice have increased risk of dermatitis

Previously, PANX3 has been implicated in either pro- or anti-inflammatory action depending on tissue expression (Halliwill et al., 2016; Pillon et al., 2014; Song et al., 2017; Wakefield et al., 2021; Zhang et al., 2019), but has so far not been investigated in unchallenged skin. Our String analysis produced two clusters related to inflammation when *Mus musculus* genes were projected to *Homo sapiens*. One String plot was found to be associated with the formation of the cornified envelope (cornification), keratinization, hair follicle morphogenesis and the hair cycle, as well as *Staphyloccocus aureus* infection (Fig. 9 A). Another cluster was associated with keratinization, and the cornified envelope, in addition to S-100 type calcium binding proteins (Fig. 9 B) which are often upregulated in psoriatic and dermatitis lesions—both of which are common inflammatory conditions of the skin (Eckert et al., 2004). Looking at relevant inflammatory genes within these

clusters such as S100 calcium binding protein A7A (*S100a7a*) and A8 (*S100a8*), dipeptidase 2 (*Dpep2*) and T cell receptor associated transmembrane adaptor 1 (*Trat1*), we found that the majority of the inflammatory gene candidates were significantly increased in the KO neonatal epidermis compared to WT (Fig. 9 C).

Since dermatitis is also common in mice, specifically of the C57BL/6 background (Hampton et al., 2012), and a compromised epidermal barrier increases the risk of skin infection, leading to inflammation and the development of dermatitis (Bozek et al., 2020; Jacoby et al., 2002), we investigated whether the increased inflammatory signalling was reflected in the incidence of dermatitis in our aging mouse colony. For this analysis we included only dermatitis cases diagnosed by the University of Western Ontario's Animal Care and Veterinary Services (ACVS) staff. ACVS used their Sick Animal Response (SAR) Treatment Algorithm for Mouse Dermatitis to diagnose each mouse, which scores dermatitis cases as a percentage based on the number of lesions, the length and character of each lesion (presence of redness, scabs and/or ulceration) and the number of times the mouse scratches in a 2-minute period (Hampton et al., 2012). An example image of a WT mouse diagnosed with moderate dermatitis (a score of 53%) is shown in Fig. 9 D. In this typical dermatitis case, the small lesion appeared red and inflamed with some evidence of scabbing. Out of a total 118 mice aged 10.5 to 18 months at the time of diagnosis, including 62 WT (22 males, 40 females) and 56 *Panx3* KO (26 males, 30 females) mice, 8 WT and 20 *Panx3* KO mice developed dermatitis (Fig. 9 E). Based on a Fisher's exact test there was an association between genotype and dermatitis incidence ($p < 0.01$), and according to the odds ratio, the risk of *Panx3* KO mice being diagnosed with dermatitis was about 3.75 times that of a WT. However, this risk differed depending on the sex of the mouse. Of the dermatitis cases, most were in female mice, with 7 WT and 14 *Panx3* KO mice developing dermatitis as opposed to only 1 WT and 6 *Panx3* KO males (Fig. 9 F). After separating the cohort based on sex, the Fisher's exact test showed an association between genotype and dermatitis diagnosis only in the female cohort ($p < 0.05$). The odds ratios also showed sex differences, with *Panx3* KO females at a 4.13 times greater risk of being diagnosed with dermatitis than female WTs, whereas *Panx3* KO males were at a 6.3 times greater risk than WT males. Thus, it seems the compromised epidermal barrier function phenotype seen in *Panx3* KO mice persists with age but there may be sex differences which would need to be investigated further in a future study.

Discussion

In this study, we found that PANX3 is a key regulator of skin homeostasis throughout aging, regulating keratinocyte adhesion, inflammation, and integrity of the epidermal barrier. When investigating the mechanism behind these functions through an expression profiling approach, we determined that the phenotypes observed in the *Panx3* KO epidermis most likely result from deficiencies in Wnt signalling and E-cadherin stabilization. Canonical Wnt signalling has been shown to play an integral role in the proliferation and differentiation of basal keratinocytes, hair follicle development and the cutaneous wound response. Non-canonical Wnt/Ca^{2+} signalling also triggers keratinocyte differentiation by stimulating intracellular Ca^{2+} release from the ER via phospholipase C activation (Lang et al., 2019). Previous research using a keratinocyte-specific KO of wntless Wnt ligand secretion mediator (WLS)—the cargo receptor for Wnt exocytosis—illustrated that the absence of Wnt secretion results in altered keratinocyte differentiation, hyperproliferation of basal keratinocytes and impairment of the epidermal barrier (Augustin et al., 2013). Thus, we speculate that the reduced Wnt signalling in *Panx3* KO neonatal epidermis

contributes to perturbations in epidermal barrier function. Using the punch biopsy wound healing model, Zhang *et al.* found that although no differences in β-catenin mRNA were seen in control versus *Panx3* KO normal skin, at the wound site, β-catenin mRNA was significantly reduced in KO compared to controls (Zhang et al., 2019). Recently, we discovered that PANX1 binds directly to β-catenin, a main player in the canonical Wnt pathway, for signalling purposes which may be independent of PANX1 channel function (Sayedyahossein et al., 2021). Thus, it is possible that PANX3 may also act as a scaffold protein to β-catenin or other Wnt signalling components, functioning through its interactome rather than as a channel protein in this instance. Since PANX3 has been shown to act as an ER Ca^{2+} leak channel in keratinocytes (Zhang et al., 2019), it is also possible that the lack of PANX3 disrupts intracellular calcium signalling and thus calcium-dependent adhesion. In the absence of PANX3 channels, reduced intracellular calcium may prevent the downstream phosphorylation of the α-, β- and p120 catenins by Src family kinases and their subsequent binding and stabilization of E-cadherin and the adherens junction complex (Bikle et al., 2012). Ultimately, resulting in the compromised barrier function exhibited in *Panx3* KO neonates. Future studies should investigate potential binding partners of PANX3 as well as elucidate its role in Wnt signalling and keratinocyte adhesion. A keratinocyte-specific *Panx3* KO mouse model should be utilized to distinctly identify the action of PANX3 in these cells, independent of external factors that exist in a global KO mouse which we recognize as a limitation of this study. In a previous report using a HaCaT PANX3-overexpression model, PANX3 was found to play a major role in keratinocyte differentiation through its channel function both intracellularly and at the plasma membrane. Furthermore, neonatal *Panx3* KO dorsal skin showed a marked reduction in the keratinocyte differentiation markers Notch1 and Epiprofin compared to controls (Zhang et al., 2021). Our findings are inconsistent with that study since we found no differences in the differentiation status of WT and *Panx3* KO neonatal epidermis, or in Notch1 or Epiprofin transcript levels in the Clariom™ S analysis. Additionally, in WT keratinocytes, *Panx3* transcripts were present at low levels but did not change with calcium-induced differentiation. However, the discrepancies seen between studies could be attributed to the use of an overexpression model as opposed to investigating the role of endogenous PANX3 in the epidermis, and the use of different global *Panx3* KO mouse models.

Despite a lack of differences in the PANX3 expression pattern between male and female dorsal skin, sex differences were observed in the histological analysis of *Panx3* KO dorsal skin of various ages. The general trend was consistent, with both the epidermal and dermal as well as hypodermal areas reduced, especially in the aged mice, but the ages in which these phenotypes were observed were sex-dependent. The reduced epidermal and dermal area observed in our *Panx3* KO mice parallels the reductions in separate epidermal and dermal thickness observed in P4 KO skin of another global *Panx3* KO mouse model. In this alternate KO model, the reduced thickness phenotypes seem to be lost by P10, based on representative images, similar to our own findings in which the reduced epidermal and dermal area was only present in P0 females and 1-year-old KO mice. Additionally, although not directly measured, the representative histological images of P4 and P38 *Panx3* KO mice illustrate a markedly reduced subcutaneous fat thickness, consistent with our findings in female KO mice, but the sexes of the analyzed mice were not reported in the study (Zhang et al., 2021). There were also some phenotypic differences observed in the skin of the two global *Panx3* KO mouse models, since the mice used by Zhang *et al*. (2021) showed reduced skin pigmentation and hair follicle numbers, not reflected in our *Panx3* KO mice which showed increased hair keratinization signalling.

Our findings are consistent with previous studies reporting on PANX3 sex differences. In a study investigating the genetic link between obesity and carcinogenesis, Halliwill *et al.* (2016) reported that *Panx3* correlated with body mass index in males but not females. Additionally, through a gene expression correlation network analysis, *Panx3* was found to be strongly associated with lipid metabolism genes such as those involved in long-chain fatty acid transport and lipid storage which was significant in both males and females (Halliwill et al., 2016). These findings could account for the reduction in subcutaneous fat seen in both male and female when *Panx3* is ablated. Furthermore, our group recently showed that adult male *Panx3* KO mice weigh less, have less overall fat and more lean mass than controls, whereas female *Panx3* KO mice weigh only slightly less than WT mice with no changes in fat or lean mass (Wakefield et al., 2021).

Since all three pannexins are expressed in the skin, there is a chance of compensation from other pannexin family members when one is ablated. Notably, PANX3 levels were significantly increased in both young and adult *Panx1* KO dorsal skin suggesting the possibility of PANX3 compensation in the absence of PANX1 (Penuela et al., 2014). However, the reciprocal cannot be said for PANX1 in *Panx3* KO mice, since we did not see any significant difference in PANX1 protein or transcript between control and *Panx3* KO dorsal skin. Although there was no protein upregulation observed, this does not rule out the possibility of functional compensation by PANX1. Phenotypically, *Panx3* KO dorsal skin has both comparable and unique properties compared to *Panx1* KO mice since both *Panx1* and *Panx3* global KO mice exhibit a reduction in the epidermal and dermal area, but unlike *Panx1* KO mice which exhibit increased subcutaneous fat, the hypodermal area is significantly reduced in the *Panx3* KO compared to WT controls (Penuela et al., 2014). We previously found that the reduction in hypodermal area in the *Panx3* KO was due to reduced adipocyte cell number rather cell size (Wakefield et al., 2021). Interestingly, the neonatal dorsal skin of the *Panx1/Panx3* double KO mouse model exhibits reduced epidermal and dermal, and increased hypodermal area like *Panx1* KO mice, but this is lost with age most likely due to functional compensation from other channel proteins in the skin (Abitbol et al., 2019). Furthermore, the PANX3 expression pattern is opposite to that seen with PANX1 in the skin, where it is highly expressed in neonatal skin but becomes downregulated in adults (Penuela et al., 2014). Since PANX1 and PANX3 are differentially regulated during skin aging, with *Panx1* and *Panx3* KO mice showing distinct skin phenotypes, these channel proteins could play opposing roles in skin formation and homeostasis. PANX2 isoform 202 was found to be downregulated in P4 *Panx3* KO dorsal skin compared to controls which is to our knowledge, the first report of a reduction in pannexin levels when another family member is ablated. It is clear that the impact of PANX3 on this PANX2 isoform occurs at the protein level, since there were no changes in *Panx2* isoform 202 transcripts between genotypes, although more investigation is needed to determine if PANX3 regulation of PANX2 occurs via expression or protein stability.

Despite the increased numbers of dermatitis in female mice, the odds ratio of developing dermatitis was much higher in male *Panx3* KO mice than in females, indicating that PANX3 plays a clear role in regulating inflammatory responses in both sexes, but the effect is more prominent in males. The overall increased dermatitis incidence in females of our aged cohort may have occurred due to multiple factors. Firstly, because females are 1.5 times more likely to barber than males (Garner et al., 2004), and in some SAR reports, ACVS staff noted that the dermatitis may be secondary to barbering. Secondly, female mice have previously been shown to be more prone to ulcerative dermatitis, an idiopathic, spontaneous and progressive form of dermatitis which is common among aged mice of the C57BL/6 background (Hampton et al., 2012). Lastly, the sample size of females in this retrospective study was 46% higher than males (70 compared to 48) which

may have also increased the overall incidence rate. These suggest higher numbers of dermatitis diagnosis in females regardless of genotype. However, a deletion of *Panx3* clearly increases the incidence of dermatitis in aged mice, suggesting a role in inflammation. Previous findings have been contradictory on the role of PANX3 in inflammation, suggesting PANX3 action may be tissue-specific. In myotubes, ATP released through palmitate-stimulated PANX3 channels was shown to be a chemoattractant for monocytes in culture, suggesting a pro-inflammatory function for PANX3 (Pillon et al., 2014). However, in pulpitis tissue, PANX3 levels were significantly reduced compared to healthy dental pulp tissue, and a dose-dependent reduction in PANX3 levels were observed when cells were stimulated with the pro-inflammatory tumour necrosis factor α (Song et al., 2017). In healthy, unchallenged dorsal skin, we found that PANX3 seems to play more of an anti-inflammatory role evidenced by its ablation increasing inflammatory signalling. Using the same global *Panx3* KO mouse model we previously showed that *Panx3* deletion reduced the inflammatory index in male visceral fat (Wakefield et al., 2021). Despite these differences, the contrary findings may not result from tissue dependence of PANX3 function, but rather age differences since visceral fat findings were in 30-week-old adult mice, whereas dermatitis cases were documented in 10.5-18-month-old aged mice. This is not the first instance of age-related effects of PANX3 since our group has previously shown the role of PANX3 in age-related acceleration of osteoarthritis (Moon et al., 2015), which contrasted the protective effects of injury-induced osteoarthritis in young mice (Moon et al., 2021).

Collectively, our findings suggest that PANX3 contributes to the maintenance of proper dorsal skin architecture, inflammatory responses and barrier function throughout aging and is critical for keratinocyte adhesion. Through the characterization of the skin of the global *Panx3* KO mouse model we discovered that PANX3 plays an integral role in the structure and function of the skin, especially within the keratinocytes. Furthermore, by understanding the role that PANX3 plays in maintaining healthy skin, we will be better equipped to identify its dysfunction in skin pathologies such as keratinocytic skin cancers like basal and squamous cell carcinomas in which PANX3 has been shown to be downregulated (Cowan et al., 2012; Halliwill et al., 2016) and may act as a tumour suppressor in malignant transformation of the skin.

Materials and methods

Animals and animal ethics

Global *Panx3* KO mice used were previously generated by our group and congenic C57BL/6N (WT) mice were used as controls (Moon et al., 2015). Mice were genotyped to verify the presence or lack of exon 2 in *Panx3* which requires two separate PCR reactions (see Table S1 for primers). After mouse euthanasia, tail tips were digested in a 0.2 mM EDTA, 25 mM NaOH solution pH 8 and then the solution was neutralized using a 40 mM Tris-HCl pH 5 solution. The Platinum® *Taq* DNA High Fidelity Polymerase (11304011; Invitrogen) and manufacturer's protocol was used for both reactions, with an annealing temperature and extension time of 58°C for 1.15 min for reaction 1 (R1) and 56°C for 1 min for reaction 2 (RT). PCR products were separated on a 1% agarose gel. R1 is used to distinguish between WTs and mice with at least one mutant allele, yielding a 1326 bp WT DNA fragment or a 600 bp DNA fragment in heterozygotes or KOs. RT distinguishes a heterozygous mouse from a full KO, where WT and heterozygous mice produce a 770 bp band, absent in a *Panx3* KO mouse. All animal experiments followed guidelines and protocols approved by the Animal Care Committee at the University of Western Ontario (#2019-069). Mice were fed Teklad 2018 (Envigo) *ad libitum* and maintained in a 12-hr-light to 12-hr-dark cycle.

Protein extraction and western blotting

Dorsal skins were dissected from WT and *Panx3* KO mice at P0, P2, P4, 4 weeks, 12 weeks, 22 weeks and 1 year, pulverized in liquid nitrogen and protein was extracted using a 1x radioimmunoprecipitation assay buffer (50mM Tris-HCl pH 8.0, 150 mM NaCl, 1% Nonidet® 40 Substitute (74385; Sigma-Aldrich), 0.5% sodium deoxycholate) containing 1 mM NaF, 1mM $Na_3VO_4 \cdot 2H_2O$ and a quarter of a Pierce™ Protease Inhibitor EDTA-free Mini Tablets (A32955; Thermo Fisher Scientific), as previously described (Abitbol et al., 2019). Protein concentrations were determined using the Pierce™ BCA Protein Assay Kit (23225; Thermo Fisher Scientific). After sample protein separation using 10% SDS-PAGE gels (40 µg per sample for all blots), membranes were transferred to a nitrocellulose membrane via the iBlot™ Gel Transfer Device (Invitrogen). Membranes were blocked overnight with 3% BSA (ALB001.100; BioShop) in 1x PBS. Blots were incubated with primary antibodies diluted in 1x PBS with 0.05% Tween20 overnight at 4°C or 1 hr at room temperature for GAPDH. Primary antibody concentrations included: anti-PANX1 CT-395 0.5 µg/mL, anti-PANX2 CT-523 4 µg/mL and anti-PANX3 CT-379 1 µg/mL (Penuela et al., 2009); generated anti-PANX3 CT-379-M1 and M2 unpurified supernatant 1:100, and anti-mouse GAPDH 0.2 µg/mL (Millipore Sigma, G8795; protein loading control). IRDye®-800CW goat anti-rabbit and -680RD goat anti-mouse IgG secondary antibodies at a 0.1 µg/mL concentration (LI-COR Biosciences, 926-32211 and 926-68070 respectively) were used for signal detection and blots were imaged on a LI-COR Odyssey Infrared Imaging System (LI-COR Biosciences). Protein levels were quantified using ImageStudio (LI-COR Biosciences), normalized to GAPDH, and presented relative to one WT mean value. For PANX1, PANX2 and PANX3 positive controls, human embryonic kidney 293T cells (HEK; CRL-3216; ATCC; RRID: CVCL_0063) were cultured in DMEM media (12430062; Gibco™) with 10% FBS (098-150; WISENT Inc), 1% penicillin/streptomycin (15140-122; Gibco™) and transfected with 5.5 µg mouse PANX1, PANX2 or PANX3 plasmids in a 10 cm plate (Penuela et al., 2007; Penuela et al., 2009) using Lipofectamine 3000 (Invitrogen) according to the manufacturer's protocol.

Generation and characterization of PANX3-specific antibodies

Carboxyl-terminal amino acid residues 379-392 (KPKHLTQHTYDEHA) of mouse PANX3 were used in mouse monoclonal antibody generation by Genemed Biotechnologies, Inc. Hybridoma supernatant from ten generated clones were tested via immunoblotting, and two clones with the highest specificity and signal intensity were selected and designated PANX3 CT-379-M1 and PANX CT-379-M2. The unpurified supernatant of PANX3 CT-379-M2 was used in the dermal fibroblast Western blot analysis alongside the previously published and characterized PANX3 CT-379 (Penuela et al., 2007). Characterization of these monoclonal antibodies by immunofluorescence (1:50 dilution) and immunoblotting (1:100 dilution) with peptide pre-adsorption as described previously (Freeman et al., 2019) is shown in Fig. 5. The peptide was pre-incubated with each antibody for 30 minutes, in 50:1 molar excess of each antibody, and ran in parallel to the antibody minus peptide conditions. For immunoblotting, IRDye®-680RD goat anti-mouse IgG secondary antibody at a 0.1 µg/mL concentration was used. Primary mouse chondrocytes were obtained from WT mice as described previously (Gosset et al., 2008), and protein was isolated as described above. For immunocytochemistry, Normal Rat Kidney (NRK; CRL-6509; ATCC; RRID: CVCL_3758) cells were plated on coverslips in a 6 well plate and transfected with 1 µg of mouse PANX3 plasmid using Lipofectamine 3000 according to the manufacturer's protocol. Forty-eight hours after transfection, cells were washed with 1x DPBS without Ca^{2+} or Mg^{2+} (14190250; Gibco™) and fixed with ice-cold methanol:acetone (5:1,

vol/vol) for 15 min at 4°C. Coverslips were blocked for 1 hr at room temperature with 10% goat serum (50062Z; Life Technologies), incubated with the primary monoclonal antibodies diluted in 1% goat serum overnight at 4°C, washed with DPBS without Ca^{2+} or Mg^{2+} and then incubated with Alexa Fluor™ 488 goat anti-mouse secondary antibody (1:700; A11029; Invitrogen) for 1 hr at room temperature. After washing, Hoechst 33342 (H3570; Life Technologies) diluted 1:1000 in double-distilled water was incubated with the samples for 5 min at room temperature to stain cell nuclei and Aqua-Mount™ (13800; Lerner Laboratories) was used to mount the coverslips. Immunofluorescence images were obtained using a ZEISS LSM 800 AiryScan Confocal Microscope from the Schulich Imaging Core Facility (University of Western Ontario) using 405 nm (Hoechst 33342) and 488 nm (Alexa Fluor 488) laser lines.

Histology and Masson's trichrome staining

Histological staining and measurements were performed on both male and female, WT and *Panx3* KO dorsal skin and paw skin of various ages as described previously (Abitbol et al., 2019). Briefly, tissue was fixed overnight at 4°C in 10% neutral-buffered formalin, processed at the Robart's Research Institute Molecular Pathology Core Facility (University of Western Ontario), embedded in paraffin and sectioned. Parallel sections (5-7 µm) were deparaffinized, rehydrated and stained with Mayer's hematoxylin (MHS16; Sigma-Aldrich) and eosin-Y (1931492; Lerner Laboratories). Stained slides were mounted using Fisher Chemical™ Permount™ Mounting Medium (SP15; Fisher Scientific) and imaged. ImageJ (Fiji) was used to crop each image to a standard frame area, manually segment and then measure the epidermal and dermal area (minus the *stratum corneum*) and hypodermal areas of the dorsal skin and the epidermal area (minus the corneal layer) of the paw skin. Four-week-old male dorsal skin sections were stained with Masson's trichrome stain following a previously reported protocol (Robb et al., 2021). Briefly, paraffin sections were deparaffinized with xylene, rehydrated in a descending ethanol series and then stained with Bouin's solution (HT10132; Sigma), Weigert's iron hematoxylin A and B (26044-05 and 26044-15; Electron Microscopy Sciences), Biebrich Scarlet-Acid Fucshin (HT151; Sigma), 10% phosphotungstic acid/10% phosphomolybdic acid (19500/19400; Electron Microscopy Sciences) and then Aniline Blue (B8563; Sigma) before incubation with 1% glacial acetic acid, ethanol dehydration and mounting (as above). Hematoxylin and eosin (H&E) and Masson's trichrome stained slides were imaged on a Leica DMIL LED brightfield inverted microscope at either 5x or 20x magnification.

Forced exercise protocol

The forced exercise protocol used is outlined previously (Wakefield et al., 2021). Briefly, 24-week-old male and female WT and *Panx3* KO mice were randomized to sedentary or forced exercise groups. Mice in the forced exercise group were forced to run on a treadmill (Columbus Instruments) for 1 h daily, 5 days per week in a 6-week period at a speed of 11 m/s and 10º incline. Then hind paws were dissected from sedentary and forced exercised mice, fixed, stained, and analyzed as above, except the paw epidermal areas were manually segmented and measured by a blind observer.

Primary dermal fibroblast and keratinocyte culture

P4 dorsal skin was dissected from WT and *Panx3* KO pups for primary dermal fibroblast and keratinocyte isolation. *Panx3* KO dermal fibroblasts were isolated using 5 cu/mL dispase (354235;

Corning) and 2 mg/mL collagenase type I (LS004196; Worthington Biochemical Corporation) treatment, cultured in DMEM media with 10% FBS and 1% penicillin/streptomycin (as above), and activated into myofibroblasts by TGF-β stimulation as previously described (Churko et al., 2011b). Briefly, 1.5 x 10^5 cells were seeded on collagen-coated 60 mm dishes and treated daily with 200 pM TGF-β1 (100-21; PeproTech) dissolved in DMEM media with 1% BSA and 1% penicillin/streptomycin for 4 days. Activation was confirmed by an increase in *Acta2* transcripts. Primary keratinocytes were isolated following the already established dispase and 0.25% trypsin/1 mM EDTA (325-043-EL; WISENT Inc.) protocol (Churko et al., 2011a), but were cultured in KGM™ Gold Keratinocyte Growth Medium BulletKit™ (192060; Lonza) on uncoated tissue culture plastic (see schematic in Fig. 7A). Trypsin was neutralized using an equal volume of 0.5 mg/mL soybean trypsin inhibitor (17075-029; Gibco™). *Panx3* KO keratinocytes were also grown on tissue culture plates coated with 50 ug/mL or 100 ug/mL rat tail type I collagen (354236; Corning), poly-D-lysine/laminin (354595; Corning) or human fibronectin (354402; Corning). Brightfield images of primary keratinocytes were taken at 20x magnification using a ZEISS Axio Vert.A1. WT keratinocytes were differentiated with 1.4 mM $CaCl_2$ treatment, confirmed by an increase in *K10* transcripts (Churko et al., 2012). For neonatal epidermis samples, the Churko *et al*. (2011a) isolation protocol was followed, except at the last step where cells would normally be cultured, un-plated epidermis samples from 4-6 pups were pooled, pelleted via centrifugation and flash frozen in liquid nitrogen for RNA isolation. Live and dead cell percentages of WT and *Panx3* KO un-plated epidermis samples were determined using the Countess™ II automated cell counter (ThermoFisher Scientific) and trypan blue (ICN1691049; Fisher Scientific).

RNA isolation and RT-qPCR

Following mouse euthanasia, P4 dorsal skin was dissected from WT and *Panx3* KO mice and immediately flash-frozen in liquid nitrogen. Ribonucleic acid (RNA) was extracted from dorsal skin using a hybrid TRIzol™ (15596018; Life Technologies) and RNeasy Plus Mini Kit (74134; Qiagen) protocol as previously described (Abitbol et al., 2019). For primary cells and neonatal epidermis, the RNeasy Plus Mini Kit (74134; Qiagen) was used for RNA extraction. Fifty ng of RNA was then reverse transcribed into cDNA using a High-Capacity cDNA Reverse Transcription Kit with RNase Inhibitor (4374966; Thermo Fisher Scientific) and following the manufacturer's instructions. Reverse transcriptase-quantitative polymerase chain reaction (RT-qPCR) was performed using SsoAdvanced Universal SYBR® Green Supermix (1725274; BioRad) according to the manufacturer's protocol. See Table S1 for a list of primers used. Samples were run in duplicate. Transcript abundance was normalized to *Gapdh*, presented as relative to one WT mean value and analyzed using the ΔΔCT method in Excel (Microsoft 365). While geometric means were represented in the graphs, logarithmic means were used to perform statistical analyses.

Epidermal barrier function assay

The epidermal barrier function of P2 WT and *Panx3* KO pups was assessed using aqueous toluidine blue staining previously described (Press et al., 2017). Pups were euthanized using CO_2, incubated briefly in ascending and then descending concentrations of methanol solutions (25%, 50%, 75%, 100%; diluted in water) and stained with 0.2% toluidine blue (89640; Sigma-Aldrich) for 15 min. After three rinses in 90% ethanol and a wash in water, pups were imaged using an iPhone SE (Apple, Inc.) and examined for blue dye permeation. Intentional barrier disruption was performed using a scalpel to make a small incision in the dorsal skin.

Dermatitis incidence

To investigate the incidence of dermatitis in an aging mouse colony we analyzed reports of dermatitis cases diagnosed by Western University's ACVS staff using their SAR Treatment Algorithm for Mouse in a blinded, retrospective cohort study (Hampton et al., 2012). A total of 118 aged mice, constituting 62 WT (22 males and 40 females) and 56 *Panx3* KO (26 males and 30 females) mice, were included in this retrospective cohort study and ranged from 10.5-18 months of age at the time of diagnosis. The number of mice in each sex and genotype diagnosed with dermatitis by a blinded veterinary assessment were counted and used to calculate the incidence of dermatitis as well as the odd's ratio of developing dermatitis. Mice were imaged using an iPhone XR (Apple, Inc.), courtesy of ACVS.

Clariom^{TM} S expression profiling and analysis

RNA from 3 pooled samples each (4-6 pups) of WT and *Panx3* KO neonatal epidermis were sent for Clariom^{TM} S, Mouse expression profiling at the Genetic and Molecular Epidemiology Laboratory at McMaster University. Expression profiling data was analyzed using TAC version 4.0.2.15 (ThermoFisher Scientific) and RStudio Cloud (https://www.rstudio.com/products/cloud/) version 4.1.2 (RStudio Team, 2022) software to find DEGs between WT and *Panx3* KO neonatal epidermis where differential expression was represented by a gene-level fold change of minimum ±1.5 and $p < 0.05$ in *Panx3* KO samples compared to controls. GSEA was used to investigate pathway-level changes by comparing the gene lists produced by Clariom S^{TM} expression profiling against *a priori* defined gene sets provided by GSEA and MSigDB C2 collection version 7.4 (Mootha et al., 2003; Subramanian et al., 2005). Enrichment Scores (ES) were generated for each gene set using a weighted Kolmogorov-Smirnov-like statistic (Subramanian et al., 2005). The ES demonstrates the degree that genes in a specific gene set are positively or negatively enriched in the *Panx3* KO neonatal epidermis compared with WT. STRING plots (https://string-db.org/) were generated using the first 100 highest ranked differentially expressed genes showing ±2-fold expression changes, setting the organism to *mus musculus* or projecting the *mus musculus* genes to *homo sapiens*, and kmeans clustering into three clusters (Szklarczyk et al., 2019; Szklarczyk et al., 2021). Reactome (https://reactome.org/) pathway analysis was also performed using minimum ±1.5-fold change gene sets with all mouse genes converted to their human-equivalent (Fabregat et al., 2016; Fabregat et al., 2017).

Statistical analysis

Statistical analyses were performed using GraphPad Prism 9 (GraphPad Software) with specific test details in each figure legend. Error bars represent mean ± SEM. All data shown is representative of three to five independent experiments or mice with two to three technical replicates, except for Fisher's exact tests for dermatitis incidence.

Acknowledgements

We would like to thank Dr. John Di Guglielmo (University of Western Ontario) for the gift of the TGF-β and Hisham Kamoun (University of Western Ontario) for his help with the Masson's trichrome staining. We would also like to thank Western University's ACVS staff for their care of the mice and providing the representative dermatitis image. Funding for this study was provided by the Natural Sciences and Engineering Research Council (NSERC) of Canada with an NSERC Discovery Grant (RGPIN-2015-06794) awarded to S. Penuela. B. O'Donnell was funded by a NSERC Postgraduate Doctoral Scholarship. The authors declare no competing financial interests.

Author contributions: B. O'Donnell conceptualized the study, completed experiments, analyzed data, and wrote the manuscript. R. Sanchez-Pupo helped with skin dissections and dermal fibroblast and keratinocyte differentiation experiments. S. Sayedyahossein performed RStudio Cloud, Reactome and STRING analysis. M. Karimi implemented computer code and supporting algorithms and applied statistical and computational techniques to analyze study data. M. Bahmani conducted the investigation process for data analysis methodology and applied statistical and computational techniques to analyze study data. C. Zhang performed the GSEA analysis and blinded forced exercise paw measurements. D. Johnston assisted with primary cell isolations and live and dead cell counts. J. Kelly completed the male dorsal skin Western blot time course. C. B. Wakefield provided the paws of the forced exercised mice. K. Barr aided in the generation of the global *Panx3* KO mouse line. L. Dagnino conceptualized the study. S. Penuela conceptualized the study, wrote and revised the manuscript, and provided funding and supervision. All authors reviewed the manuscript.

Abbreviations

Acta2, (mRNA)– alpha smooth muscle actin (α-SMA) transcript
ACVS – Animal Care and Veterinary Services
Atp5me, (mRNA)– ATP synthase subunit E transcript
C57BL/6N – C57 Black 6 Mouse Strain N
Cdh1, (mRNA)– Cadherin 1 transcript
DEGs – Differentially Expressed Genes
EMT – Epithelial to Mesenchymal Transition
ES – Enrichment Scores
GSEA – Gene Set Enrichment Analysis
HEK – Human Embryonic Kidney
Inv, (mRNA) – Involucrin transcript
K#, (mRNA) – Keratin # transcript
Lor, (mRNA) – Loricrin transcript
Lrp5, (mRNA) – Low-density lipoprotein receptor-related protein 5 transcript
KO – Knockout
M# – Monoclonal #
MSigDB – Molecular Signatures Database
Ndufa1, (mRNA) – NADH dehydrogenase (ubiquinone) 1 alpha subcomplex subunit 1 transcript
P# – Post-partum day #
PANX1/*Panx1*/(mRNA) *Panx1* – Pannexin 1 protein/gene/transcript
PANX2/(mRNA) *Panx2* – Pannexin 2 protein/transcript
PANX3/*Panx3*/(mRNA) *Panx3* – Pannexin 3 protein/gene/transcript
R1 – Reaction 1
RT – Reaction 2
REK – Rat Epidermal Keratinocyte
SAR – Sick Animal Response
TAC – Transcriptome Analysis Software
Vcl, (mRNA) – Vinculin transcript
Wnt3, (mRNA) – Wnt family member 3 transcript
WT – Wildtype

References

Abitbol, J., B. O'Donnell, W. CB, E. Jewlal, J. Kelly, K. Barr, K. Willmore, B. Allman, and S. Penuela. 2019. Double deletion of Panx1 and Panx3 affects skin and bone but not hearing. *J Mol Med*. 97:723-726.

Augustin, I., J. Gross, D. Baumann, C. Korn, G. Kerr, T. Grigoryan, C. Mauch, W. Birchmeier, and M. Boutros. 2013. Loss of epidermal Evi/Wls results in a phenotype resembling psoriasiform dermatitis. *J Exp Med*. 210:1761-1777.

Bao, L., S. Locovei, and G. Dahl. 2004. Pannexin membrane channels are mechanosensitive conduits for ATP. *FEBS Letters*. 572:65-68.

Baroni, A., E. Buommino, V. De Gregorio, E. Ruocco, V. Ruocco, and R. Wolf. 2012. Structure and function of the epidermis related to barrier properties. *Clin Dermatol*. 30:257-262.

Bikle, D., Z. Xie, and C. Tu. 2012. Calcium regulation of keratinocyte differentiation. *Expert Rev Endocrinol Metab*. 7:461-472.

Binnerts, M.E., K.A. Kim, J.M. Bright, S.M. Patel, K. Tran, M. Zhou, J.M. Leung, Y. Liu, W.E. Lomas, 3rd, M. Dixon, S.A. Hazell, M. Wagle, W.S. Nie, N. Tomasevic, J. Williams, X. Zhan, M.D. Levy, W.D. Funk, and A. Abo. 2007. R-Spondin1 regulates Wnt signaling by inhibiting internalization of LRP6. *Proc Natl Acad Sci U S A*. 104:14700-14705.

Bond, S.R., A. Lau, S. Penuela, A.V. Sampaio, T.M. Underhill, D.W. Laird, and C.C. Naus. 2011. Pannexin 3 is a novel target for Runx2, expressed by osteoblasts and mature growth plate chondrocytes. *J Bone Miner Res*. 26:2911-2922.

Bozek, A., M. Zajac, and M. Krupka. 2020. Atopic Dermatitis and Psoriasis as Overlapping Syndromes. *Mediators Inflamm*. 2020:7527859.

Bragulla, H.H., and D.G. Homberger. 2009. Structure and functions of keratin proteins in simple, stratified, keratinized and cornified epithelia. *J Anat*. 214:516-559.

Celetti, S.J., K.N. Cowan, S. Penuela, Q. Shao, J. Churko, and D.W. Laird. 2010. Implications of pannexin 1 and pannexin 3 for keratinocyte differentiation. *J Cell Sci*. 123:1363-1372.

Chekeni, F.B., M.R. Elliott, J.K. Sandilos, S.F. Walk, M. Kinchen, E.R. Lazarowski, A.J. Armstrong, S. Penuela, W. Laird, G.S. Salvesen, B.E. Isakson, D.a. Bayliss, and S. Kodi. 2011. Pannexin 1 channels mediate 'find–me' signal release and membrane permeability during apoptosis. *Nature*. 467:863-867.

Churko, J., J. Chan, Q. Shao, and D. Laird. 2011a. The G60S Connexin43 Mutant Regulates Hair Growth and Hair Fiber Morphology in a Mouse Model of Human Oculodentodigital Dysplasia. *J Invest Dermatol*. 131:2197–2204.

Churko, J., J. Chan, Q. Shao, and D. Laird. 2012. The G60S Cx43 mutant enhances keratinocyte proliferation and differentiation. *Exp Dermatol*. 21:612-618.

Churko, J., Q. Shao, X. Gong, K. Swoboda, D. Bai, J. Sampson, and D.W. Laird. 2011b. Human Dermal Fibroblasts Derived from Oculodentodigital Dysplasia Patients Suggest that Patients may have Wound Healing Defects. *Hum Mutat*. 32:456-466.

Cowan, K.N., S. Langlois, S. Penuela, B.J. Cowan, and D.W. Laird. 2012. Pannexin1 and Pannexin3 Exhibit Distinct Localization Patterns in Human Skin Appendages and are Regulated during Keratinocyte Differentiation and Carcinogenesis. *Cell Commun Adhes*. 19:45-53.

Eckert, R.L., A.M. Broome, M. Ruse, N. Robinson, D. Ryan, and K. Lee. 2004. S100 proteins in the epidermis. *J Invest Dermatol*. 123:23-33.

Fabregat, A., K. Sidiropoulos, P. Garapati, M. Gillespie, K. Hausmann, R. Haw, B. Jassal, S. Jupe, F. Korninger, S. McKay, L. Matthews, B. May, M. Milacic, K. Rothfels, V. Shamovsky,

M. Webber, J. Weiser, M. Williams, G. Wu, L. Stein, H. Hermjakob, and P. D'Eustachio. 2016. The Reactome pathway Knowledgebase. *Nucleic Acids Res*. 44:D481-487.

Fabregat, A., K. Sidiropoulos, G. Viteri, O. Forner, P. Marin-Garcia, V. Arnau, P. D'Eustachio, L. Stein, and H. Hermjakob. 2017. Reactome pathway analysis: a high-performance in-memory approach. *BMC Bioinformatics*. 18:142.

Freeman, T.J., S. Sayedyahossein, D. Johnston, R.E. Sanchez-Pupo, B. O'Donnell, K. Huang, Z. Lakhani, D. Nouri-Nejad, K.J. Barr, L. Harland, S. Latosinsky, A. Grant, L. Dagnino, and S. Penuela. 2019. Inhibition of Pannexin 1 Reduces the Tumorigenic Properties of Human Melanoma Cells. *Cancers (Basel)*. 11.

Fu, D., F. Song, H. Sun, D. Pei, Y. Wang, J. Lei, and C. Huang. 2015. Expression of Pannexin3 in human odontoblast-like cells and its hemichannel function in mediating ATP release. *Arch Oral Biol*. 60:1510-1516.

Garg, N., A. Gerstner, V. Bhatia, J. Deford, and J. Papaconstantinou. 2004. Gene expression analysis in mitochondria from chagasic mice: alterations in specific metabolic pathways. *Biochem J*. 381:743-752.

Garner, J.P., S.M. Weisker, B. Dufour, and J.A. Mench. 2004. Barbering (Fur and Whisker Trimming) by Laboratory Mice as a Model of Human Trichotillomania and Obsessive-Compulsive Spectrum Disorders. *Comp Med*. 54:216-224.

Gosset, M., F. Berenbaum, S. Thirion, and C. Jacques. 2008. Primary culture and phenotyping of murine chondrocytes. *Nat Protoc*. 3:1253-1260.

Halliwill, K., D. Quigley, H. Chung Kang, R. Del Rosario, D. Ginzinger, and A. Balmain. 2016. Panx3 links body mass index and tumorigenesis in a genetically heterogeneous mouse model of carcinogen-induced cancer. *Genome Med*. 8:83-100.

Hampton, A.L., G.A. Hish, M.N. Aslam, E.D. Rothman, I.L. Bergin, K.A. Patterson, M. Naik, T. Paruchuri, J. Varani, and H.G. Rush. 2012. Progression of Ulcerative Dermatitis Lesions in C57BL/6Crl Mice and the Development of a Scoring System for Dermatitis Lesions. *J Am Assoc Lab Anim Sci*. 51:586-593.

Hartsock, A., and W.J. Nelson. 2008. Adherens and tight junctions: structure, function and connections to the actin cytoskeleton. *Biochim Biophys Acta*. 1778:660-669.

Holmen, S.L., T.A. Giambernardi, C.R. Zylstra, B.D. Buckner-Berghuis, J.H. Resau, J.F. Hess, V. Glatt, M.L. Bouxsein, M. Ai, M.L. Warman, and B.O. Williams. 2004. Decreased BMD and limb deformities in mice carrying mutations in both Lrp5 and Lrp6. *J Bone Miner Res*. 19:2033-2040.

Ishikawa, M., T. Iwamoto, S. Fukumoto, and Y. Yamada. 2014. Pannexin 3 inhibits proliferation of osteoprogenitor cells by regulating Wnt and p21 signaling. *J Biol Chem*. 289:2839-2851.

Ishikawa, M., T. Iwamoto, T. Nakamura, A. Doyle, S. Fukumoto, and Y. Yamada. 2011. Pannexin 3 functions as an ER Ca 2+ channel, hemichannel, and gap junction to promote osteoblast differentiation. *J Cell Biol*. 193:1257-1274.

Ishikawa, M., G. Williams, P. Forcinito, M. Ishikawa, R.J. Petrie, K. Saito, S. Fukumoto, and Y. Yamada. 2019. Pannexin 3 ER Ca(2+) channel gating is regulated by phosphorylation at the Serine 68 residue in osteoblast differentiation. *Sci Rep*. 9:18759.

Iwamoto, T., T. Nakamura, A. Doyle, M. Ishikawa, S. De Vega, S. Fukumoto, and Y. Yamada. 2010. Pannexin 3 regulates intracellular ATP/cAMP levels and promotes chondrocyte differentiation. *J Biol Chem*. 285:18948-18958.

Jacoby, R.O., J.G. Fox, and M. Davisson. 2002. Biology and Diseases of Mice. *In* Laboratory Animal Medicine. 35–120.

Lang, C.M.R., C.K. Chan, A. Veltri, and W.H. Lien. 2019. Wnt Signaling Pathways in Keratinocyte Carcinomas. *Cancers (Basel)*. 11.

Langlois, S., X. Xiang, K. Young, B.J. Cowan, S. Penuela, and K.N. Cowan. 2014. Pannexin 1 and pannexin 3 channels regulate skeletal muscle myoblast proliferation and differentiation. *J Biol Chem*. 289:30717-30731.

Le Vasseur, M., J. Lelowski, J. Bechberger, W. Sin, and C.C. Naus. 2014. Pannexin 2 protein expression is not restricted to the CNS. *Front Cell Neurosci*. 8.

Locovei, S., J. Wang, and G. Dahl. 2006. Activation of pannexin 1 channels by ATP through P2Y receptors and by cytoplasmic calcium. *FEBS Lett*. 580:239-244.

Lohman, A.W., M. Billaud, S.A. C, S.R. Johnstone, A. Best, M. Lee, K. Barr, S. Penuela, D.W. Laird, and B.E. Isakson. 2012. Expression of Pannexin Isoforms in the Systemic Murine Arterial Network. *J Vasc Res*. 49:405-416.

Moon, P.M., S. Penuela, K. Barr, S. Khan, C.L. Pin, I. Welch, M. Attur, S.B. Abramson, D.W. Laird, and F. Beier. 2015. Deletion of Panx3 Prevents the Development of Surgically Induced Osteoarthritis. *J Mol Med*. 93:845-856.

Moon, P.M., Z.Y. Shao, G. Wambiekele, C. Appleton, D.W. Laird, S. Penuela, and F. Beier. 2021. Global Deletion of Pannexin 3 Accelerates Development of Aging-induced Osteoarthritis in Mice. *Arthritis Rheumatol*.

Mootha, V.K., C.M. Lindgren, K. Eriksson, A. Subramanian, S. Sihag, J. Lehar, P. Puigserver, E. Carlsson, M. Ridderstråle, E. Laurila, N. Houstis, M.J. Daly, N. Patterson, J.P. Mesirov, T.R. Golub, P. Tamayo, B. Spiegelman, E.S. Lander, J.N. Hirschhorn, D. Altshuler, and L.C. Groop. 2003. PGC-1α-responsive genes involved in oxidative phosphorylation are coordinately downregulated in human diabetes. *Nat Genet*. 34:267-273.

O'Donnell, B.L., and S. Penuela. 2021. Pannexin 3 channels in health and disease. *Purinergic Signal*. 17:577-589.

Panchin, Y., I. Kelmanson, M. Matz, K. Lukyanov, N. Usman, and S. Lukyanov. 2000. A ubiquitous family of putative gap junction molecules. *Curr Biol*. 10:473-474.

Pelegrin, P., and A. Surprenant. 2006. Pannexin-1 mediates large pore formation and interleukin-1β release by the ATP-gated P2X7 receptor. *EMBO J*. 25:5071-5082.

Penuela, S., R. Bhalla, X.-Q. Gong, K.N. Cowan, S.J. Celetti, B.J. Cowan, D. Bai, Q. Shao, and D.W. Laird. 2007. Pannexin 1 and pannexin 3 are glycoproteins that exhibit many distinct characteristics from the connexin family of gap junction proteins. *J Cell Sci*. 120:3772-3783.

Penuela, S., R. Bhalla, K. Nag, and D. Laird. 2009. Glycosylation Regulates Pannexin Intermixing and Cellular Localization. *Mol Biol Cell*. 20:4313–4323.

Penuela, S., J.J. Kelly, J.M. Churko, K.J. Barr, A.C. Berger, and D.W. Laird. 2014. Panx1 Regulates Cellular Properties of Keratinocytes and Dermal Fibroblasts in Skin Development and Wound Healing. *J Invest Dermatol*. 134:2026-2035.

Pillon, N., Y. Li, L. Fink, J. Brozinick, J. Nikolayev, M. Kuo, P. Bilan, and A. Klip. 2014. Nucleotides Released From Palmitate-Challenged Muscle Cells Through Pannexin-3 Attract Monocytes. *Diabetes*. 63:3815-3826.

Piprek, R.P., M. Kolasa, D. Podkowa, M. Kloc, and J.Z. Kubiak. 2019. Tissue-specific knockout of E-cadherin (Cdh1) in developing mouse gonads causes germ cells loss. *Reproduction*. 158:147-157.

Press, E., K. Alaga, K. Barr, Q. Shao, F. Bosen, K. Willecke, and D. Laird. 2017. Disease-linked connexin26 S17F promotes volar skin abnormalities and mild wound healing defects in mice. *Cell Death Dis*. 8:e2845.

Robb, K.P., L. Juignet, P. Morissette Martin, J.T. Walker, C.R. Brooks, C. Barreira, G.A. Dekaban, and L.E. Flynn. 2021. Adipose Stromal Cells Enhance Decellularized Adipose Tissue Remodeling Through Multimodal Mechanisms. *Tissue Eng Part A*. 27:618-630.

RStudio Team. 2022. RStudio: Integrated Development Environment for R. RStudio, PBC, Boston, MA.

Sanchez-Pupo, R.E., B.L. O'Donnell, D. Johnston, L. Gyenis, D.W. Litchfield, and S. Penuela. 2022. Pannexin 2 is expressed in murine skin and promotes UVB-induced apoptosis of keratinocytes. *Mol Biol Cell*. 33:1-14.

Sayedyahossein, S., K. Huang, Z. Li, C. Zhang, A.M. Kozlov, D. Johnston, D. Nouri-Nejad, L. Dagnino, D.H. Betts, D.B. Sacks, and S. Penuela. 2021. Pannexin 1 binds beta-catenin to modulate melanoma cell growth and metabolism. *J Biol Chem*:100478.

Schmidt, M., D. Gutknecht, J. Simon, J. Schulz, B. Eckes, U. Anderegg, and A. Saalbach. 2015. Controlling the Balance of Fibroblast Proliferation and Differentiation: Impact of Thy-1. *J Invest Dermatol*. 135:1893–1902.

Smack, D.P., B.P. Korge, and W.D. James. 1994. Keratin and keratinization. *J Am Acad Dermatol*. 30:85-102.

Song, F., H. Sun, Y. Wang, H. Yang, L. Huang, D. Fu, J. Gan, and C. Huang. 2017. Pannexin3 inhibits TNF-alpha-induced inflammatory response by suppressing NF-kappaB signalling pathway in human dental pulp cells. *J Cell Mol Med*. 21:444-455.

Soro-Arnaiz, I., Q.O.Y. Li, M. Torres-Capelli, F. Melendez-Rodriguez, S. Veiga, K. Veys, D. Sebastian, A. Elorza, D. Tello, P. Hernansanz-Agustin, S. Cogliati, J.M. Moreno-Navarrete, E. Balsa, E. Fuertes, E. Romanos, A. Martinez-Ruiz, J.A. Enriquez, J.M. Fernandez-Real, A. Zorzano, K. De Bock, and J. Aragones. 2016. Role of Mitochondrial Complex IV in Age-Dependent Obesity. *Cell Rep*. 16:2991-3002.

Subramanian, A., P. Tamayo, V.K. Mootha, S. Mukherjee, B.L. Ebert, M.A. Gillette, A. Paulovich, S.L. Pomeroy, T.R. Golub, E.S. Lander, and J.P. Mesirov. 2005. Gene set enrichment analysis: a knowledge-based approach for interpreting genome-wide expression profiles. *Proc Natl Acad Sci U S A*. 102:15545-15550.

Szklarczyk, D., A.L. Gable, D. Lyon, A. Junge, S. Wyder, J. Huerta-Cepas, M. Simonovic, N.T. Doncheva, J.H. Morris, P. Bork, L.J. Jensen, and C.V. Mering. 2019. STRING v11: protein-protein association networks with increased coverage, supporting functional discovery in genome-wide experimental datasets. *Nucleic Acids Res*. 47:D607-D613.

Szklarczyk, D., A.L. Gable, K.C. Nastou, D. Lyon, R. Kirsch, S. Pyysalo, N.T. Doncheva, M. Legeay, T. Fang, P. Bork, L.J. Jensen, and C. von Mering. 2021. The STRING database in 2021: customizable protein-protein networks, and functional characterization of user-uploaded gene/measurement sets. *Nucleic Acids Res*. 49:D605-D612.

Turmel, P., J. Dufresne, L. Hermo, C.E. Smith, S. Penuela, D.W. Laird, and D.G. Cyr. 2011. Characterization of pannexin1 and pannexin3 and their regulation by androgens in the male reproductive tract of the adult rat. *Mol Reprod Dev*. 78:124-138.

Valenta, T., G. Hausmann, and K. Basler. 2012. The many faces and functions of beta-catenin. *EMBO J*. 31:2714-2736.

Wakefield, C.B., V.R. Lee, D. Johnston, P. Boroumand, N.J. Pillon, S. Sayedyahossein, B.L. O'Donnell, J. Tang, R.E. Sanchez-Pupo, K.J. Barr, R. Gros, L. Flynn, N.M. Borradaile, A.

Klip, F. Beier, and S. Penuela. 2021. Pannexin 3 deletion reduces fat accumulation and inflammation in a sex-specific manner. *International Journal of Obesity*.

Wikramanayake, T.C., O. Stojadinovic, and M. Tomic-Canic. 2014. Epidermal Differentiation in Barrier Maintenance and Wound Healing. *Adv Wound Care (New Rochelle)*. 3:272-280.

Ye, J., G. Coulouris, I. Zaretskaya, I. Cutcutache, S. Rozen, and T.L. Madden. 2012. Primer-BLAST: A tool to design target-specific primers for polymerase chain reaction. *BMC Bioinformatics*. 13:134.

Zhang, P., M. Ishikawa, A. Doyle, T. Nakamura, B. He, and Y. Yamada. 2021. Pannexin 3 regulates skin development via Epiprofin. *Sci Rep*. 11:1779.

Zhang, P., M. Ishikawa, C. Rhodes, A. Doyle, T. Ikeuchi, K. Nakamura, Y. Chiba, B. He, and Y. Yamada. 2019. Pannexin-3 deficiency delays skin wound healing in mice due to defects in channel functionality. *J Invest Dermatol*. 139:909-918.

Figure Legends

Figure 1. **PANX3 is expressed in mouse dorsal skin beginning at P2, with the same protein expression pattern seen in both sexes. A representative i**mmunoblot showing the presence of PANX3 in both male **(A)** and female **(B)** mouse dorsal skin from P4 to 1 year of age, with a significant increase in PANX3 levels from P0 to P4 ($N = 3$, $p = 0.0004$ for males; $N = 4$, $p = 0.0013$ for females). **(C)** In female WT mice, PANX3 levels gradually increase from P0 to P4 ($N = 4$, $p < 0.0001$). Human embryonic kidney 293 cells ectopically expressing a mouse PANX3 plasmid (HEK + PANX3) were used as a positive control. All blots were probed with the polyclonal PANX3 CT-379 antibdy. PANX3 levels normalized to GAPDH (protein loading control) and compared using a one-way ordinary measures ANOVA followed by Tukey's multiple comparisons test. Protein sizes in kDa and error bars indicate SEM.

Figure 2. **In male *Panx3* KO mice dorsal skin, the hypodermal area is decreased at 4 weeks and 1 year compared to WT mice with the epidermal and dermal area also reduced at 1 year.** Histological analysis of male murine dorsal skin at various ages showed the hypodermal area at 4 weeks ($p < 0.0001$) and 1 year of age ($p = 0.0003$) was significantly decreased in *Panx3* KO mice compared to age-matched WT mice (unpaired t-test). The epidermal and dermal area of 1-year-old *Panx3* KO mice was also reduced ($p = 0.0091$). No significant differences were seen in either epidermal and dermal or hypodermal areas at any other age (NS, $p > 0.05$). The upper brackets represent the epidermal and dermal layers (minus the *stratum corneum*) and the lower brackets represent the hypodermis. $N = 5$, $n = 15$ for all timepoints and genotypes. Error bars represent SEM. Scale bars represent 50 µm at P0, 100 µm at P4, 4 weeks, 22 weeks and 1 year. NS, no significance.

Figure 3. **In female *Panx3* KO mice dorsal skin, the hypodermal area is consistently reduced compared to WT controls, whereas an epidermal and dermal area reduction is seen only at P0 and 1 year.** Histological analysis of female murine dorsal skin at various ages showed a decreased hypodermal area from P0 to 1 year in *Panx3* KO mice compared to WT mice of the same age (P0 $p < 0.0001$; P4 $p = 0.0297$; 4 weeks $p = 0.0226$; 22 weeks $p = 0.0001$; 1 year $p = 0.0032$; unpaired t-test). A reduction in epidermal and dermal area was seen in P0 ($p = 0.01$) and 1-year-old ($p = 0.0408$) *Panx3* KO dorsal skin. No significant differences were seen in epidermal and dermal areas at any other age (NS, $p > 0.05$). $N = 5$, $n = 15$ for all timepoints and genotypes.

The upper brackets represent the epidermal and dermal layers (minus the *stratum corneum*) and the lower brackets represent the hypodermis. Error bars represent SEM. Scale bars represent 50 μm at P0, 100 μm at P4, 4 weeks, 22 weeks and 1 year. NS, no significance.

Figure 4. **PANX3 is undetectable in P4 WT dermal fibroblasts. (A)** Dermal area measurements from P0 and P4 timepoints of both male and female dorsal skin from the histological analysis samples in Figure 2 and 3 (N = 5). The dermal area was significantly reduced in P0 *Panx3* KO female dorsal skin compared to age-matched WTs (p = 0.0057), but unchanged in all other measurements (NS, no significance; unpaired t-test). **(B)** Protein levels of PANX3 were assessed in WT and *Panx3* KO dermal fibroblasts isolated from P4 dorsal skin (N = 6 for each genotype) using both monoclonal anti-PANX3 CT-379-M2 and polyclonal PANX3 CT-379 antibodies, but no PANX3 protein was detected. GAPDH was used as a protein loading control and HEK + PANX3 were used as a positive control, protein sizes in kDa. **(C)** Transcript levels of (mRNA) *Panx3* were assessed in WT fibroblasts in either control or TGF-β conditions. *Panx3* KO fibroblasts were used as a negative control for *Panx3* transcript levels. There were no differences seen in (mRNA) *Panx3* in control and TGF-β conditions (N = 3, $p > 0.05$; one-way ordinary measures ANOVA). NS, no significance. Fibroblasts were activated by 200 pM of TGF-β stimulation for 4 days in serum free media supplemented with 1% BSA. Activation was confirmed by an increase in α-smooth muscle actin (*Acta2*) transcript (p = 0.0167, paired t-test). *Gapdh* was used to calculate normalized mRNA expression using the ΔΔCT method. Bars represent mean ± SEM. **(D)** Masson's Trichrome staining of 4-week-old male WT and *Panx3* KO mouse dorsal skin show similar levels of collagen abundance. Histological staining (H & E) also shown for reference. N = 3, scale bar represents 100 μm.

Figure 5. **Epidermal barrier function is compromised in neonatal *Panx3* KO dorsal skin. (A)** *Panx3* transcript levels were assessed in WT and *Panx3* KO neonatal epidermis isolated from P4 dorsal skin to confirm respective genotypes. N = 3 of pooled samples of 4-6 pups per genotype. Gapdh was used to calculate normalized mRNA expression using the ΔΔCT method. **(B)** Epidermal area measurements from P0 and P4 timepoints of both male and female dorsal skin from the histological samples shown in Figure 2 and 3 (N = 5). The epidermal areas of each genotype were not significantly different in any timepoints and sexes ($p > 0.05$; NS, no significance; unpaired t-test). **(C)** P2 male and female WT and *Panx3* KO pups were subjected to toluidine blue staining to test for epidermal barrier function. Blue dye infiltration seen in all *Panx3* KO pups, but not in unstained controls or WT pups, is indicative of compromised barrier function. Intentional barrier disruption was performed using a scalpel (Cut) to make a small incision in the dorsal skin as a control. Arrows point to areas of increased dye infiltration in the mouth, nose, paw and tails of *Panx3* KO mice and corresponding areas in WT pups for comparison. N = 5 per sex per genotype from three separate experiments.

Figure 6. **Analysis of WT and *Panx3* KO neonatal epidermis Clariom™ S expression profiling data. (A)** Schematic (Created with Biorender.com) showing the isolation of primary keratinocytes and neonatal epidermis from P4 pup skin. Dorsal skin is dissected from pups and incubated with dispase to allow for the separation of the epidermis from the underlying dermal and hypodermal layers which are discarded. After trypsin digestion of the epidermis to break up cell contacts, primary keratinocytes can be plated, or the neonatal epidermis can be pooled from multiple pups (4-6) and flash frozen in liquid nitrogen for subsequent RNA isolation. **(B)** Transcriptomic analysis

of WT and *Panx3* KO P4 neonatal epidermis ($N = 3$) was conducted using Clariom™ S expression profiling and analyzed by RStudio Cloud software. A principal component analysis was used to visualize differences in the expression of the first fifty highest ranked genes and the two genotypes are separated. Each circle represents an individual neonatal epidermis sample. **(C)** Heat map showing the first 30 highest ranked differentially expressed genes between WT (WT1–3) and *Panx3* KO (KO1–3) neonatal epidermis. Individual genes found to have a gene-level fold change of minimum ±2 column Z-score and $p < 0.05$ between WT and *Panx3* KO samples. **(D)** Major functional categories and signalling pathways affected by *Panx3* ablation in neonatal epidermis and the corresponding gene candidates identified to have altered expression in *Panx3* KO samples compared to WT controls.

Figure 7. **Keratinization signalling is positively enriched in *Panx3* KO neonatal epidermis, but differentially expressed genes function in forming and maintaining the epidermal barrier rather than in keratinocyte differentiation. (A)** Transcriptomic differences between *Panx3* KO and WT neonatal epidermis were evaluated using GSEA. Enrichment plots were generated using the MSigDB C2 collection: Canonical Pathways consisting of 22 206 genes in 2922 gene sets. After ranking, the most positively enriched gene sets in *Panx3* KO neonatal epidermis (Enrichment Score, ES > 0) included the Keratinization pathway. Green lines represent changes in ES per identified gene in the gene set. Vertical black lines on the red portion of the gradient represent genes positively enriched in *Panx3* KO samples, while black lines on the blue portion of the gradient represent genes negatively enriched in KO samples. **(B)** Undifferentiated (*K14, K5*) and differentiated (*Inv, Lor*) keratinocyte markers were analyzed in WT and *Panx3* KO neonatal epidermis via RT-qPCR ($N = 3$). No differences were seen between genotypes in any of the markers ($p > 0.05$, unpaired t-test). *Gapdh* was used to calculate normalized mRNA expression using the ΔΔCT method. Bars represent mean ± SEM. NS, no significance. **(C)** *Panx3* transcript levels were assessed in cultured WT keratinocytes in either control or Ca^{2+} conditions. No differences were seen in (mRNA) *Panx3* ($p > 0.05$). Keratinocytes were differentiated by 1.4 mM $CaCl_2$ stimulation, confirmed by an increase in *K10* transcript ($p = 0.0012$). $N = 4$, paired t-test. *Gapdh* was used to calculate normalized mRNA expression using the ΔΔCT method. Bars represent mean ± SEM. NS, no significance. **(D)** A STRING plot was generated using the first 100 highest ranked differentially expressed genes showing ±2-fold expression changes, organism *Mus musculus* and kmeans clustering into three clusters. This cluster is associated with keratinization, epidermis morphogenesis and formation of the cornified envelope. Red nodes represent query proteins and the first shell of interactors. Empty nodes represent proteins of unknown 3D structure, whereas filled nodes have some 3D structure known or predicted. Edges represent protein-protein associations: teal from curated databases, fuchsia pink were experimentally determined, yellow from textmining, black shows co-expression, and periwinkle blue represents protein homology. **(E)** Log epithelial splicing regulatory protein 2 (*Esrp2*), late cornified envelope 1m (*Lce1m*), cornifin-B (*Sprr1b*) and filaggrin 2 (*Flg2*) expression normalized and presented relative to the WT average. *Espr2* and *Lce1m* transcript levels were significantly reduced in *Panx3* KO samples compared to WT (**$p < 0.01$), and although not significant (mRNA) *Sprr1b* and *Flg2* levels trended to a decrease in KO neonatal epidermis. Unpaired t-test, bars represent mean ± SEM.

Figure 8. **Adhesion signalling is reduced in *Panx3* KO neonatal epidermis and primary *Panx3* KO keratinocytes do not adhere in culture. (A)** Transcriptomic differences between *Panx3* KO and WT neonatal epidermis were evaluated using GSEA. Enrichment plots were generated

using the MSigDB C2 collection: Canonical Pathways consisting of 22 206 genes in 2922 gene sets. After ranking, E-cadherin stabilization and Wnt signalling pathways were the gene sets with the largest negative enrichment in *Panx3* KO neonatal epidermis (ES < 0). Green lines represent changes in ES per identified gene in the gene set. Vertical black lines on the red portion of the gradient represent genes positively enriched in *Panx3* KO samples, while black lines on the blue portion of the gradient represent genes negatively enriched in *Panx3* KO samples. **(B)** Transcript levels of multiple markers from the E-cadherin and Wnt signalling gene sets were compared to confirm Clariom™ S findings. Vinculin (*Vcl*, $p = 0.0042$), Wnt family member 3 (*Wnt3*, $p = 0.0083$) and low-density lipoprotein receptor-related protein 5 (*Lrp5*, $p = 0.0064$) were significantly reduced in *Panx3* KO neonatal epidermis. Cadherin 1 (*Cdh1*, $p = 0.08$), although not significantly different between genotypes, showed a trend to reduced levels in the KO neonatal epidermis. $N = 3$, unpaired t-test. *Gapdh* was used to calculate normalized mRNA expression using the ΔΔCT method. Bars represent mean ± SEM. **(C)** Brightfield images of WT and *Panx3* KO primary keratinocytes cultured on untreated tissue culture plastic at day 7 and day 3 respectively. Scale bar represents 50 µm, images taken at 20X. **(D)** Live and dead cell percentages of WT and *Panx3* KO neonatal epidermis samples were not significantly different (NS, unpaired t-test) between genotypes. $N = 9$ individual pups per genotype. **(E)** Brightfield images of *Panx3* KO keratinocytes isolated from P4 dorsal skin and plated on tissue culture plastic coated with either 50 µg/mL collagen, 100 µg/mL collagen, laminin or fibronectin. $N = 6$ per condition. Scale bar represents 50 µm.

Figure 9. **The incidence of dermatitis is more common in aged *Panx3* KO mice than WT but shows sex-specific differences.** STRING plots were generated using the first 100 highest ranked differentially expressed genes showing ±2-fold expression changes, projecting the *Mus musculus* genes to *Homo sapiens* and kmeans clustering into three clusters. Cluster **(A)** is associated with keratinization, cornification, hair follicle morphogenesis, formation of the cornified envelope and *Staphylococcus aureus* infection. Cluster **(B)** is associated with keratinization, the cornified envelope and S-100/ICaBP type calcium binding domain, often upregulated in psoriatic lesions. Red nodes represent query proteins and the first shell of interactors. Empty nodes represent proteins of unknown 3D structure, whereas filled nodes have some 3D structure known or predicted. Edges represent protein-protein associations: teal from curated databases, fuchsia pink were experimentally determined, yellow from textmining, black shows co-expression, and periwinkle blue represents protein homology. **(C)** Log S100 calcium binding protein A7A (*S100a7a*), S100 calcium binding protein A8 (*S100a8*), dipeptidase 2 (*Dpep2*) and T cell receptor associated transmembrane adaptor 1 (*Trat1*) expression normalized and presented relative to the WT average (set as 1). *S100a7a*, *S100a8*, *Dpep2*, and *Trat1* transcript levels were significantly increased in *Panx3* KO samples compared to WT (*$p < 0.05$, **$p < 0.01$). Unpaired t test, bars represent mean ± SEM. **(D)** Image of a WT female mouse aged 13.5 months with dermatitis, lesion denoted by white arrow, identified as having a dermatitis score of 53% using Western University's ACVS SAR Treatment Algorithm for Mouse Dermatitis. **(E)** The incidence of dermatitis was calculated in a cohort of aging WT and *Panx3* KO mice. A total of 62 WT (22 males, 40 females) and 56 *Panx3* KO (26 males, 30 females) mice were included. SAR case reports from a blinded veterinary assessment of our colony were referenced and the number of mice with confirmed cases of dermatitis, were counted and analyzed. For total mice from each genotype, the analysis was statistically significant with a $p < 0.01$, showing an association between genotype and dermatitis incidence. **(F)** The incidence of dermatitis in each sex was calculated in the same cohort mice.

Seven cases of dermatitis were diagnosed in the males (1 WT and 6 *Panx3* KO), but there was no association between a dermatitis diagnosis and the genotype in the male cohort (p = 0.11). However, there were 21 cases of dermatitis in female mice (7 WT and 14 *Panx3* KO), and an association between dermatitis diagnosis and mouse genotype (p = 0.02). Mouse age at the time of dermatitis diagnosis ranged from 10.5–18 months. Fisher's exact test.

Table 1. **List of genotyping and RT-qPCR primers.**

Primer	Forward Sequence (5' – 3')	Reverse Sequence (5' – 3')	Reference
Panx3 R1 (Genotyping)	CGCAGCATTCCGGAACCTGAG	AACTAGCCGGAGGGGTCG	(Abitbol et al., 2019)
Panx3 RT (Genotyping)	CGCAGCATTCCGGAACCTGAG	CTTGTCCTGCGTATGGTG	(Abitbol et al., 2019)
Panx3	TTTCGCCCAGGAGTTCTCATC	CCTGCCTGACACTGAAGTTG	(Abitbol et al., 2019)
Panx1	ACAGGCTGCCTTTGTGGATTCA	GGGCAGGTACAGGAGTATG	(Abitbol et al., 2019)
Panx2 Full Length	TGGTACCCATCCTGCTGGT	GGGTGAAGTTGTGCGGAGT	(Abitbol et al., 2019)
Panx2 Isoform 202	CAGCCCGTGTCTCCTCTCTAC	GTAGCCGCGGGCGTACA	(Abitbol et al., 2019)
Gapdh	TGCGACTTCAACAGCAACTC	GTAGGCCATGAGGTCCAC	(Abitbol et al., 2019)
Acta2 (α-SMA)	GCTGGACTCTGGAGATGG	GCAGTAGTCACGAAGGAATAG	(Schmidt et al., 2015)
K14	AGTGAGAAAGTGACCATGCAGA	CTGCCAGGATCTTGCTCTTCAG	(Ye et al., 2012)
K5	TGAGGAGCTGCAACAGACAG	AGGTTGGCACACTGCTTCTT	(Ye et al., 2012)
Inv	CTCCTGTGAGTTTGTTTGGTCT	CACACAGTCTTGAGAGGTCCC	(Ye et al., 2012)
Lor	TCCCTGGTGCTTCAGGGTAAC	TCTTTCCACAACCCACAGGA	(Ye et al., 2012)
K10	CAGCTGGCCCTGAAACAATC	AGTTGTTGGTACTCGGCGTT	(Ye et al., 2012)
Cdh1	CCCAAGCACGTATCAGGGTC	GTACACAGCTTTCCACGCC	(Piprek et al., 2019)
Vcl	TGGTCTAGCAAGGGCAATGA	AAAGCCAGCATCTGTTCGGA	(Ye et al., 2012)
Wnt3	CAAGCACAACAATGAAGCAGG	TCGGGACTCACGGTGTTTCTC	(Binnerts et al., 2007)
Lrp5	TGTACTGCAGCTTGGTCCC	CCAGTAAATGTCGGAGTCTACAATG	(Holmen et al., 2004)
Cox5b	GGAGATCATGATAGCAGCACAGA	AGCTGCCTTTGGAGGTAGCA	(Soro-Arnaiz et al., 2016)
Atp5me	CGGTTCAGGTCTCTCCACTC	TGCTGTCATCTTGAGCTTCC	(Garg et al., 2004)
Ndufa1	GGGTTGGCGTGCGAGTAAC	CAACTCGTTTTTCCTTGCCCC	(Ye et al., 2012)

Figure 1

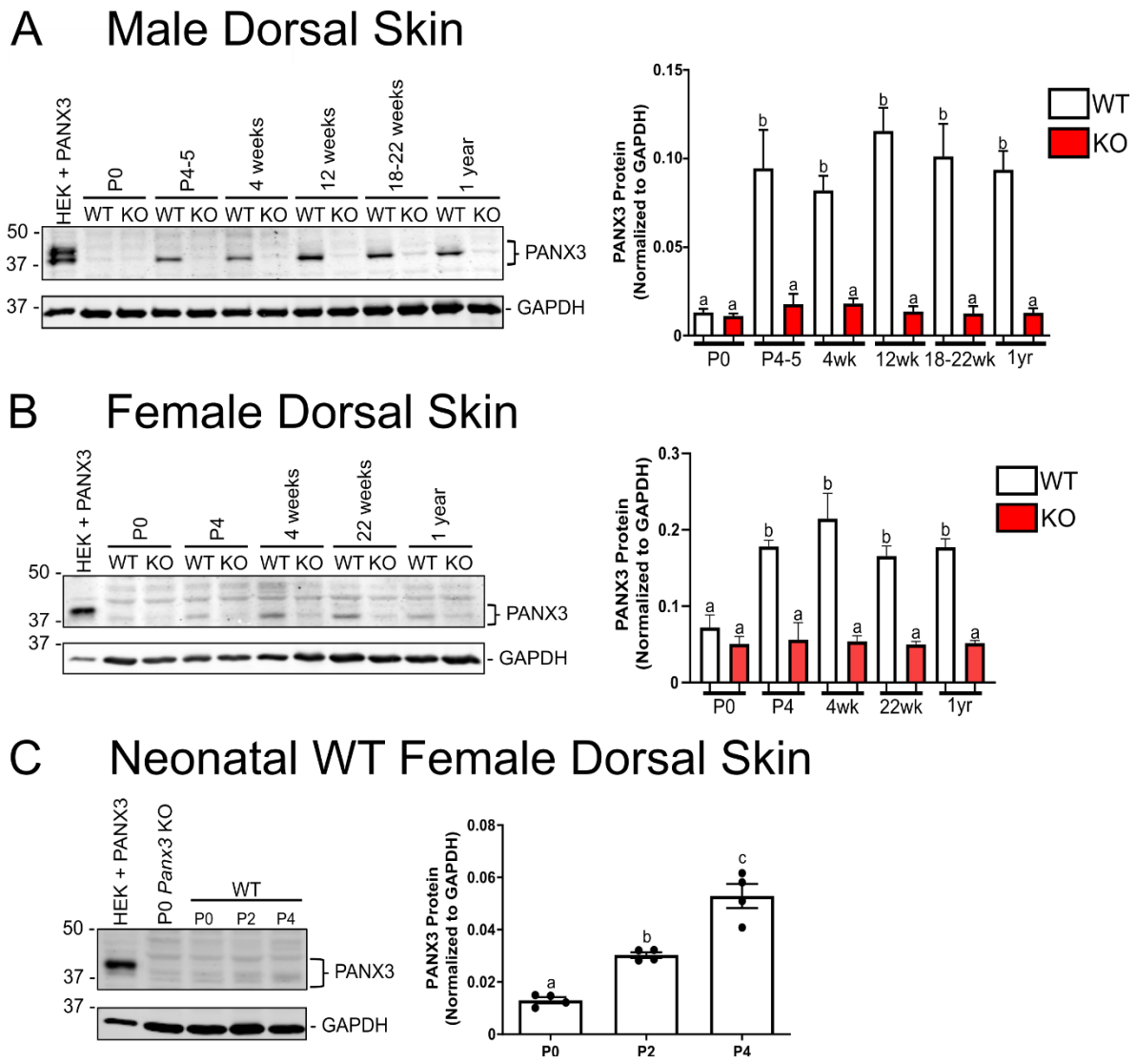
A Male Dorsal Skin
HEK + PANX3
P0
P4-5
4 weeks
12 weeks
18-22 weeks
1 year
WT KO WT KO WT KO WT KO WT KO WT KO
50
37
37
PANX3
GAPDH
PANX3 Protein (Normalized to GAPDH)
0.15
0.10
0.05
0
WT
KO
P0
P4-5
4wk
12wk
18-22wk
1yr
B Female Dorsal Skin
HEK + PANX3
P0
P4
4 weeks
22 weeks
1 year
WT KO WT KO WT KO WT KO WT KO
50
37
37
PANX3
GAPDH
PANX3 Protein (Normalized to GAPDH)
0.3
0.2
0.1
0
WT
KO
P0
P4
4wk
22wk
1yr
C Neonatal WT Female Dorsal Skin
HEK + PANX3
P0 Panx3 KO
WT
P0 P2 P4
50
37
37
PANX3
GAPDH
PANX3 Protein (Normalized to GAPDH)
0.08
0.06
0.04
0.02
0
P0
P2
P4

Figure 2

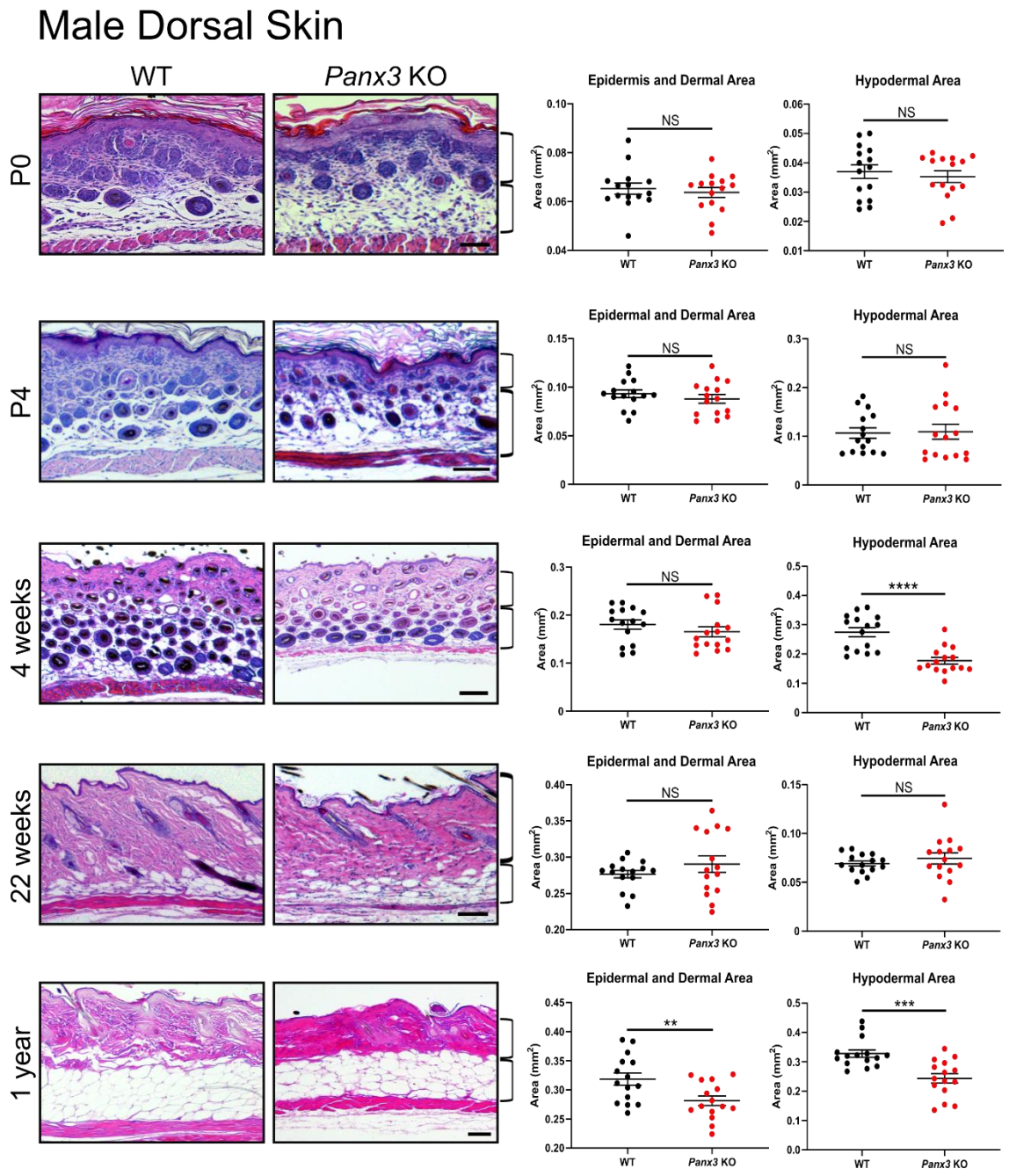
Male Dorsal Skin
WT
Panx3 KO
P0
P4
4 weeks
22 weeks
1 year
Epidermis and Dermal Area
Epidermal and Dermal Area
Hypodermal Area
Area (mm²)
NS
**
***
****
WT
Panx3 KO

Figure 3

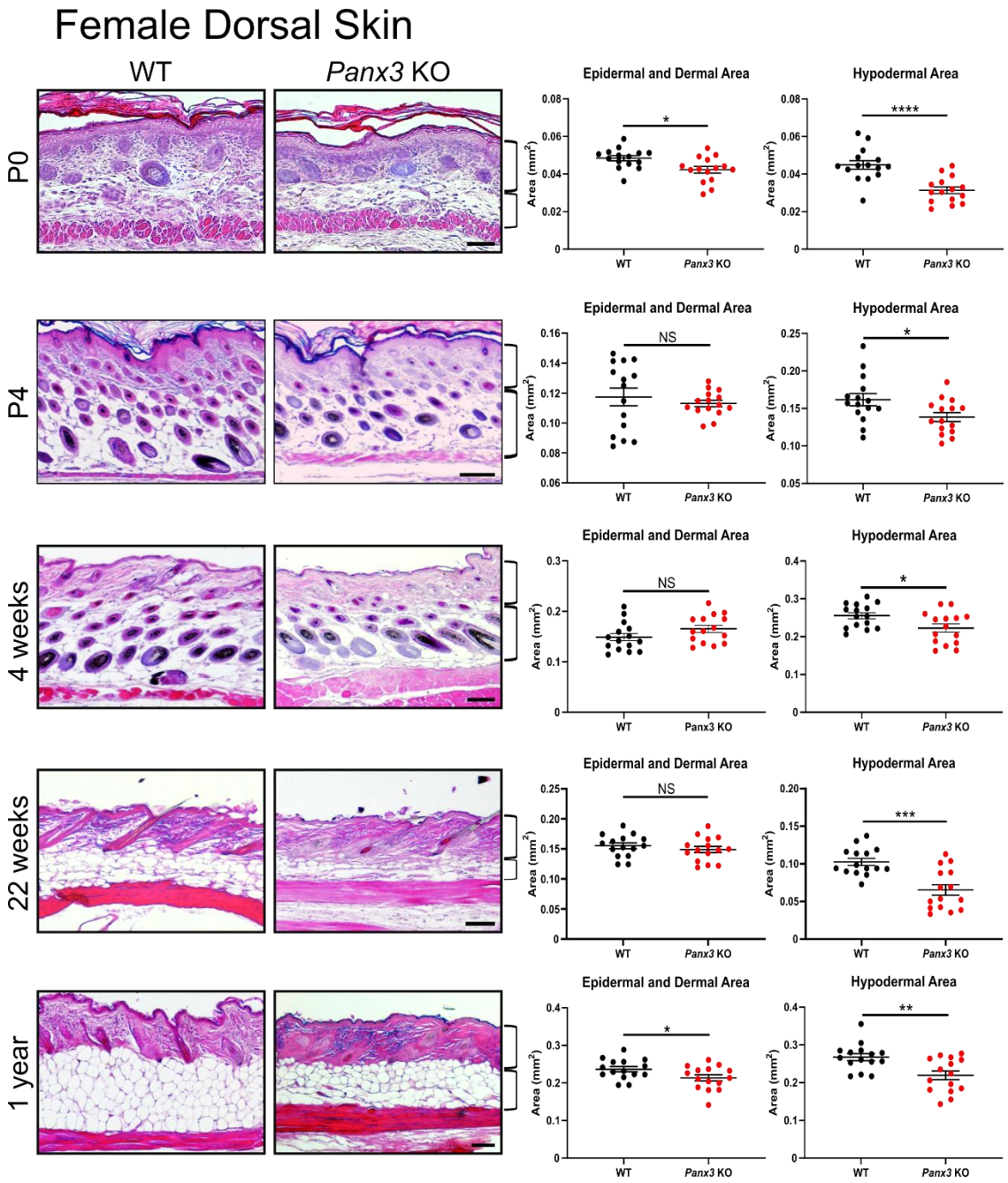
Female Dorsal Skin
WT
Panx3 KO
P0
P4
4 weeks
22 weeks
1 year
Epidermal and Dermal Area
Hypodermal Area
Area (mm²)
WT
Panx3 KO
*
****
NS
*
NS
*
NS
***
*
**

Figure 4

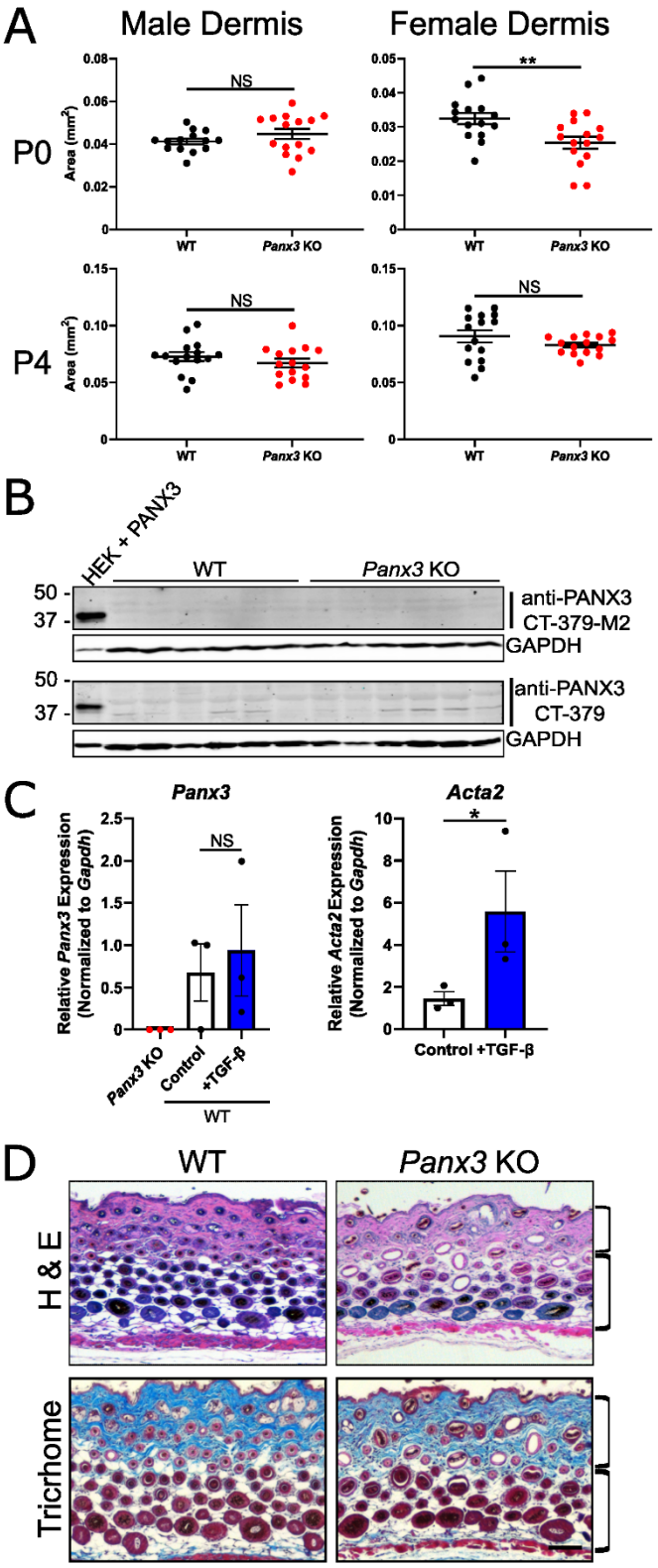
A
Male Dermis
Female Dermis
P0
P4
Area (mm²)
NS
**
WT
Panx3 KO
B
HEK + PANX3
WT
Panx3 KO
50
37
anti-PANX3 CT-379-M2
GAPDH
anti-PANX3 CT-379
C
Panx3
Acta2
Relative Panx3 Expression (Normalized to Gapdh)
Relative Acta2 Expression (Normalized to Gapdh)
Panx3 KO
Control
+TGF-β
Control +TGF-β
D
H & E
Tricrhome

Figure 5

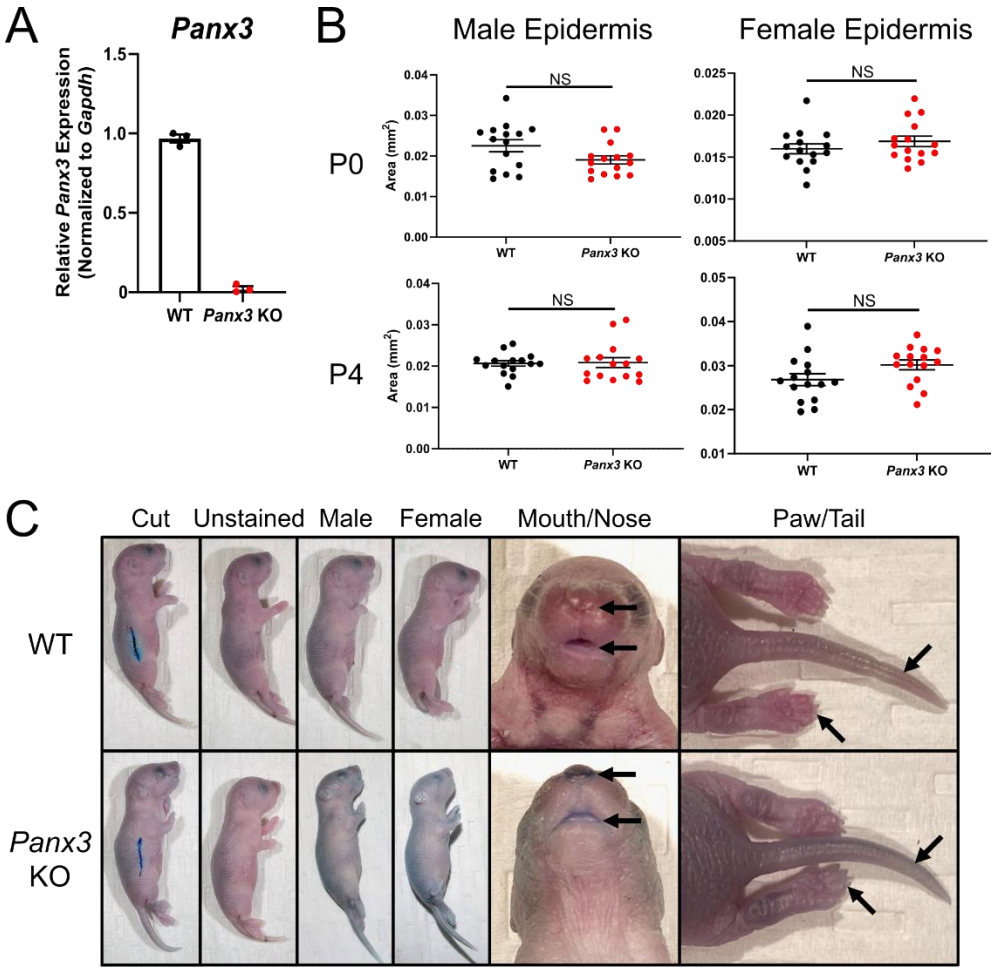
A
Panx3
Relative Panx3 Expression (Normalized to Gapdh)
1.5
1.0
0.5
0
WT
Panx3 KO
B
Male Epidermis
Female Epidermis
P0
P4
Area (mm²)
NS
WT
Panx3 KO
C
Cut
Unstained
Male
Female
Mouth/Nose
Paw/Tail
WT
Panx3 KO

Figure 6

A

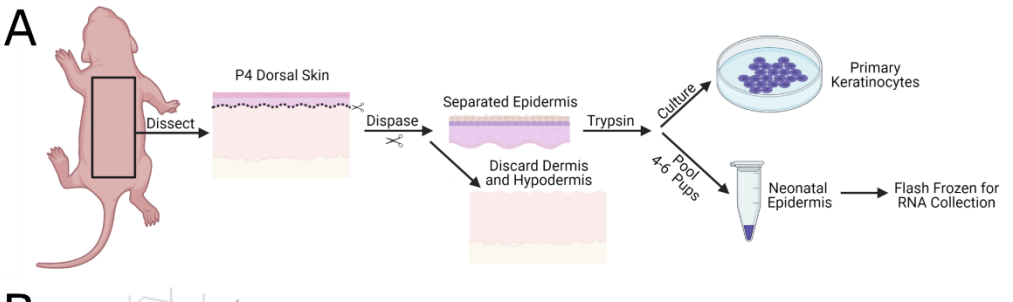

B

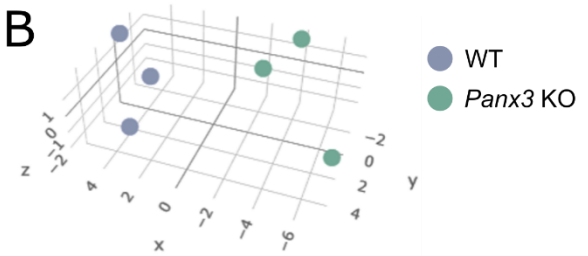

C

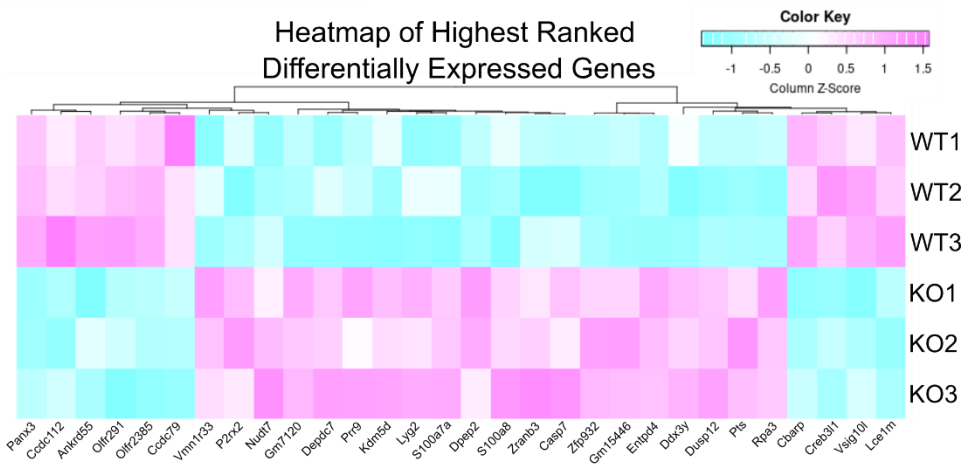

D

Functional Category/Signalling Pathway	Gene Candidates with Altered Expression
Skin Development	*Stmn1, Casp7, Rptn, Krtap5-4, Entpd4*
Hair Follicles	*Stmn1, Lyg2, Casp7, Wfdc18, Fgfr1, Krtap4-8, Krt71, Tchh*
Wound Healing	*Gprc5a, Pts, Dpep2, Itm2a*
Barrier Function	*Esrp2, Lce1m, Stmn1, Sprr1b, Dgat2, Flg2, Elovl1*
Differentiation	*Arhgap32, Sh3kbp1, Cops3, Lce1m, Cpsf41, B9d1, Pts, Cyp2u1, Dynlt1, Rab4a, S100a7a, Sprr1b, H2afv, Krtap5-4*
Proliferation	*Rnf7, Rpa3, Pts, Cyp2u1, Stmn1, Lyg2, Pisd-ps3, Tchhl1, Tbca*
Cell-Cell and Cell-Matrix Adhesion	*Sh3kbp1, Cops3, Lrrc4c, Zmat3, Rab4a, Pard6a, Spink5, P3h2, Col6a4*
Inflammation, Psoriasis, Atopic Dermatitis and Infection	*Rgs1, Tsc22d3, Trat1, Il1rap, Dpep2, Il1r2, Pfdn4, Il18r1, S100a7a, Dpep2, P2rx2, S100a8, Casp7, Zranb3, Ccdc112, Cd207, Gm4553, Ltb4r2, Fabp4, Nlrp4e, Gas7, Crnn, Itm2a, Hpse, Atf3, Klk13, Gm19402, Lyz2, Irf1, Cbarp, Nudt7, Ankrd55, Lyg2*
Migration and Invasion	*Dynlt1, Gprc5a, Stmn1, Il1r2, Rpa3, Tm4sf1*
Metabolism	*Polr2h, Cox7a2l*
SCC	*Polr2h, Sh3kbp1, S100a7a, Fgfr1, Tchhl1*
Hedgehog Signalling	*Zfp932, B9d1, Pard6a*
Wnt/E-cadherin Signalling	*Il1r2, Pard6a, Arhgap32, Gpr137*
Smad Signalling	*Il1r2, Cdc42ep3*

Figure 7

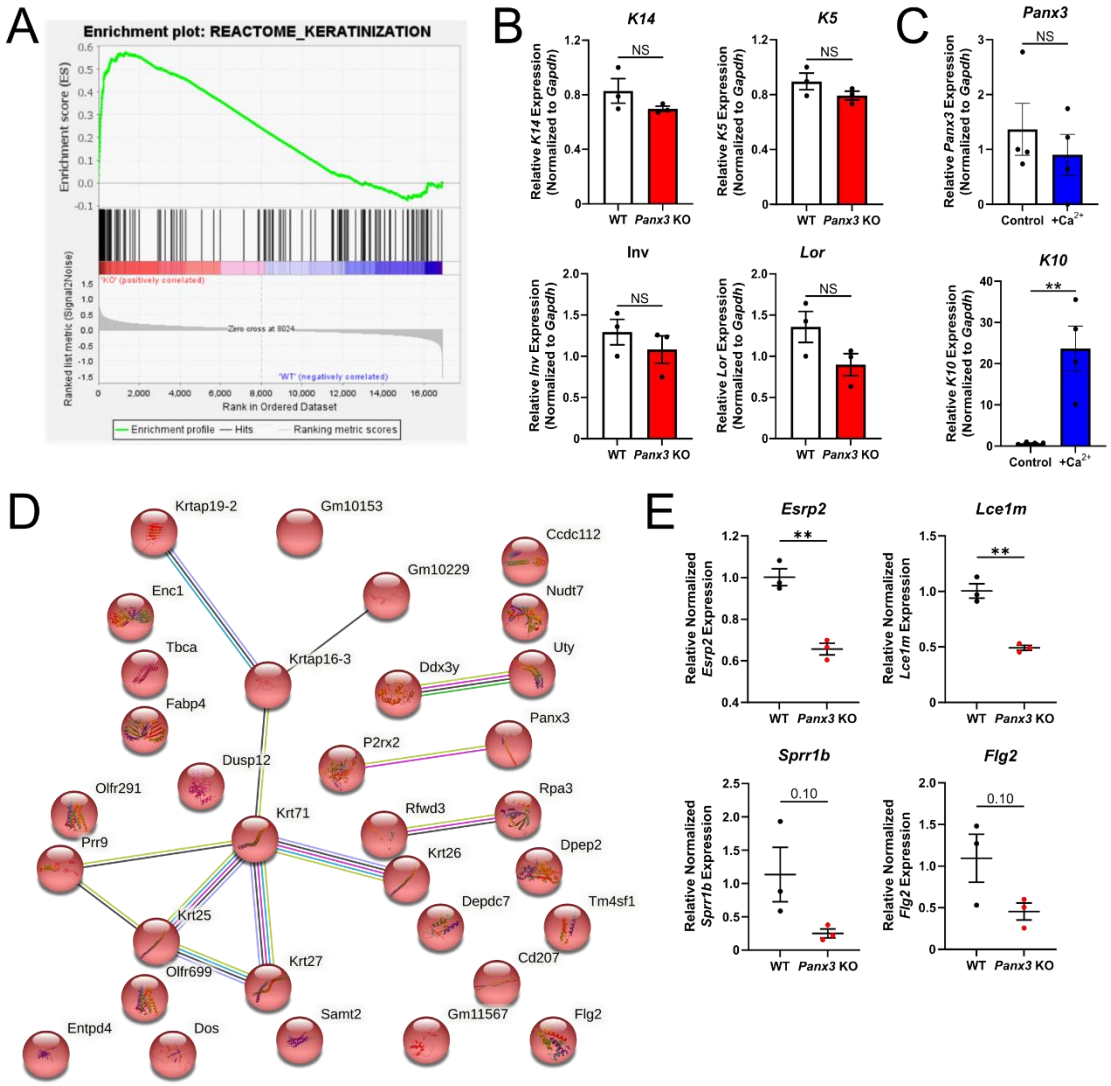
A
Enrichment plot: REACTOME_KERATINIZATION
Enrichment score (ES)
'KO' (positively correlated)
Zero cross at 8024
'WT' (negatively correlated)
Ranked list metric (Signal2Noise)
Rank in Ordered Dataset
Enrichment profile
Hits
Ranking metric scores
B
K14
K5
Inv
Lor
NS
Relative K14 Expression (Normalized to Gapdh)
Relative K5 Expression (Normalized to Gapdh)
Relative Inv Expression (Normalized to Gapdh)
Relative Lor Expression (Normalized to Gapdh)
WT
Panx3 KO
C
Panx3
K10
NS
**
Relative Panx3 Expression (Normalized to Gapdh)
Relative K10 Expression (Normalized to Gapdh)
Control
+Ca2+
D
Krtap19-2
Gm10153
Ccdc112
Gm10229
Nudt7
Enc1
Tbca
Krtap16-3
Ddx3y
Uty
Fabp4
Panx3
P2rx2
Dusp12
Olfr291
Rpa3
Rfwd3
Krt71
Prr9
Krt26
Dpep2
Depdc7
Tm4sf1
Krt25
Cd207
Olfr699
Krt27
Samt2
Gm11567
Flg2
Entpd4
Dos
E
Esrp2
Lce1m
Sprr1b
Flg2
**
0.10
Relative Normalized Esrp2 Expression
Relative Normalized Lce1m Expression
Relative Normalized Sprr1b Expression
Relative Normalized Flg2 Expression
WT
Panx3 KO

Figure 8

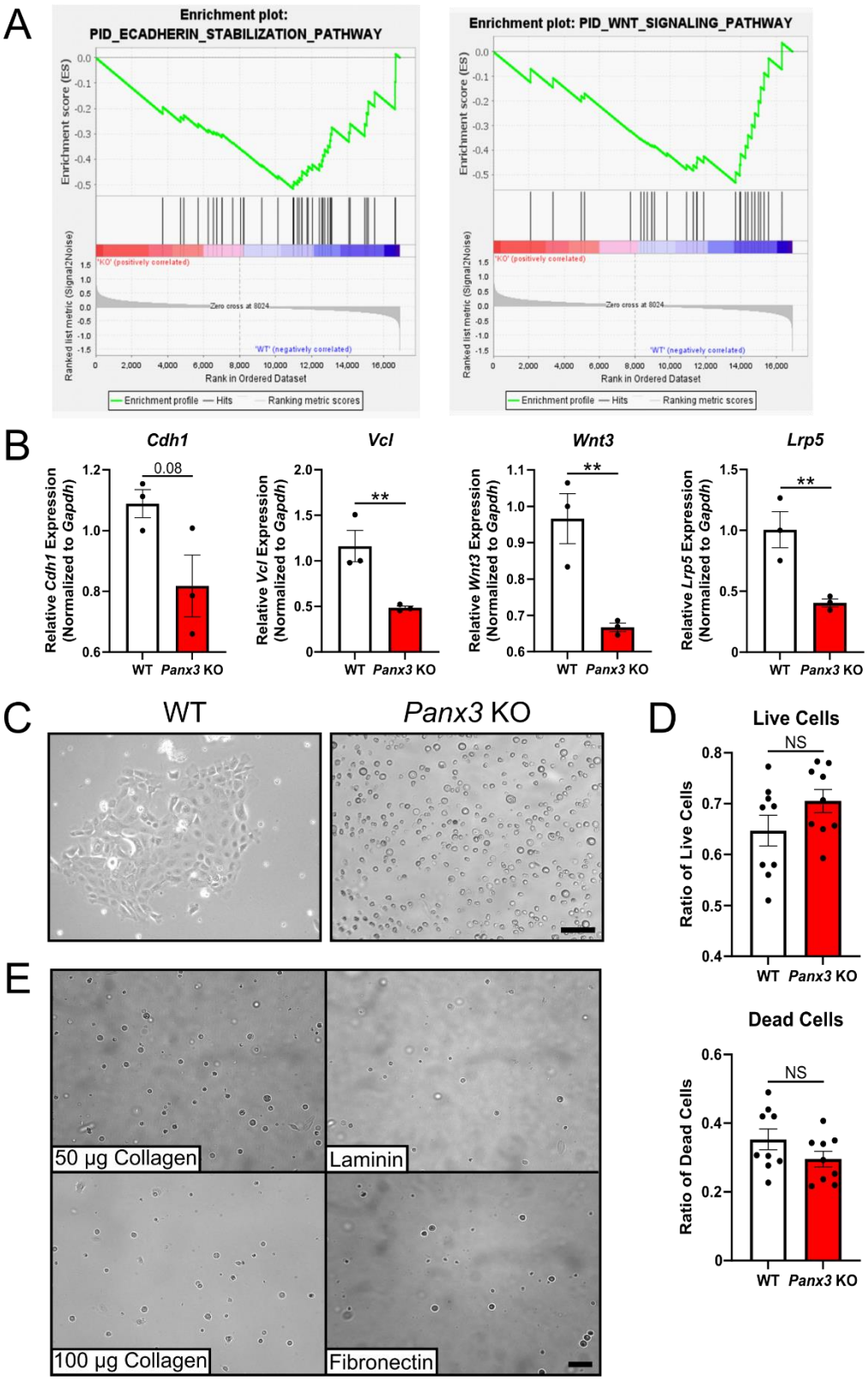
A
Enrichment plot: PID_ECADHERIN_STABILIZATION_PATHWAY
Enrichment plot: PID_WNT_SIGNALING_PATHWAY
Enrichment score (ES)
Ranked list metric (Signal2Noise)
'KO' (positively correlated)
Zero cross at 8024
'WT' (negatively correlated)
Rank in Ordered Dataset
Enrichment profile
Hits
Ranking metric scores
B
Cdh1
Vcl
Wnt3
Lrp5
Relative Cdh1 Expression (Normalized to Gapdh)
Relative Vcl Expression (Normalized to Gapdh)
Relative Wnt3 Expression (Normalized to Gapdh)
Relative Lrp5 Expression (Normalized to Gapdh)
0.08
**
WT
Panx3 KO
C
WT
Panx3 KO
D
Live Cells
NS
Ratio of Live Cells
Dead Cells
Ratio of Dead Cells
E
50 µg Collagen
Laminin
100 µg Collagen
Fibronectin

Figure 9

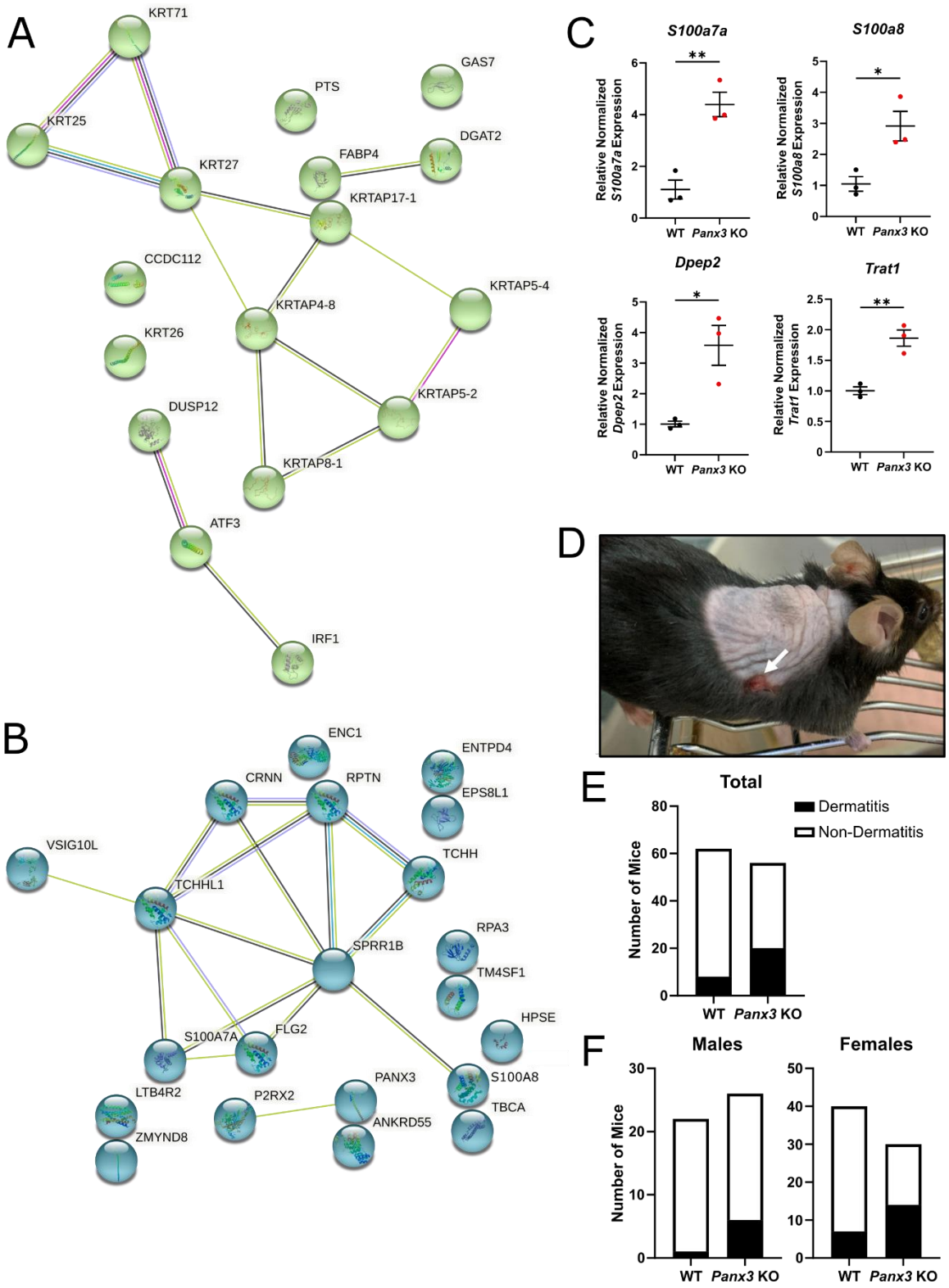
A
KRT71
GAS7
PTS
KRT25
DGAT2
FABP4
KRT27
KRTAP17-1
CCDC112
KRTAP5-4
KRTAP4-8
KRT26
KRTAP5-2
DUSP12
KRTAP8-1
ATF3
IRF1
B
ENC1
ENTPD4
CRNN
RPTN
EPS8L1
VSIG10L
TCHH
TCHHL1
RPA3
SPRR1B
TM4SF1
HPSE
S100A7A
FLG2
PANX3
S100A8
LTB4R2
P2RX2
TBCA
ANKRD55
ZMYND8
C
S100a7a
S100a8
Dpep2
Trat1
Relative Normalized S100a7a Expression
Relative Normalized S100a8 Expression
Relative Normalized Dpep2 Expression
Relative Normalized Trat1 Expression
WT
Panx3 KO
D
E
Total
Dermatitis
Non-Dermatitis
Number of Mice
F
Males
Females